An extended Chain and Trinuclear Complexes Based on Pt(II)–M (M = Tl(I), Pb(II)) Bonds: Contrasting Photophysical Behaviour

Juan Forniés,[a] Nora Giménez,[b] Susana Ibáñez,[a,c] Elena Lalinde,[b] Antonio Martín,* [a] and M. Teresa Moreno* [b]

[a] *Departamento de Química Inorgánica - Instituto de Síntesis Química y Catálisis Homogénea. Universidad de Zaragoza - C.S.I.C. 50009 Zaragoza, Spain*

[b]*Departamento de Química-Centro de Síntesis Química de La Rioja, (CISQ), Universidad de La Rioja, 26006, Logroño, Spain.*

[c] *Present Address: Dpto. de Química Inorgánica y Orgánica, Universitat Jaume I Avda. Vicente Sos Baynat s/n, 12071, Castellón, Spain.*

A. M: e-mail: tello@unizar.es

M. T. M. E-mail: teresa.moreno@unirioja.es

Abstract

The synthesis and structural characterization of a Pt-Tl chain $[\{Pt(bzq)(C_6F_5)_2\}Tl(Me_2CO)]_n$ **1** and two trinuclear Pt_2M clusters $(NBu_4)[\{Pt(bzq)(C_6F_5)_2\}_2Tl]$ **2** and $[\{Pt(bzq)(C_6F_5)_2\}_2Pb]$ **3**, stabilized by donor-acceptor Pt→M bonds, is reported. The 1D heterometallic chain **1** is formed by alternate "$Pt(bzq)(C_6F_5)_2$" and "$Tl(Me_2CO)$" fragments, with Pt-Tl bond separations in the range 2.961(1)-3.067(1) Å. The isoelectronic trinuclear complexes **2** (which crystallizes in three forms **2a**, **2b** and **2c**) and **3** present a sandwich structure in which the Tl(I) or Pb(II) is located between two "$Pt(bzq)(C_6F_5)_2$" subunits. NMR studies suggest equilibria in solution implying cleavage and reformation of Pt-M bonds. The lowest-lying absorption band in the UV-vis spectra in CH_2Cl_2 and THF of **1**, associated to ^{1}MLCT/^{1}L´LCT $^1[5d_\pi(Pt)\rightarrow\pi^*(bzq)]/^1[(C_6F_5)\rightarrow bzq]$, displays a blue shift in relation to the precursor, suggesting the cleavage of the chain maintaining bimetallic Pt-Tl

fragments in solution, also supported by NMR spectroscopy. In **2** and **3**, it shows a blue-shift in THF and a red-shift in CH_2Cl_2, supporting a more extensive cleavage of the Pt-M bonds in THF solutions than in CH_2Cl_2, where the trinuclear entities are predominant. The Pt-Tl chain **1** displays in solid state a bright orange-red emission ascribed to ^{3}MM'CT (M' = Tl). It exhibits remarkable and fast reversible vapochromic and vapoluminescent response to donor vapors (THF and Et_2O), related to the coordination/decoordination of the guest molecule to the Tl(I) ion, and mechanochromic behaviour, associated to the shortening of the intermetallic Pt-Tl separations in the chain induced by grinding. In frozen solutions (THF, acetone and CH_2Cl_2) **1** shows interesting luminescence thermochromism with emissions strongly dependent on the solvent, concentration and excitation wavelengths. The Pt_2Tl complex **2** shows an emission close to **1**, ascribed to charge transfer from the platinum fragment to the thallium [^{3}(L+L')MM'CT]. **2** also shows vapoluminescent behaviour in presence of vapors of Me_2CO, THF and Et_2O, although smaller and slower than in **1**. The trinuclear neutral complex Pt_2Pb **3** displays a blue-shift emission band, tentatively assigned to admixture of ^{3}MM'CT ^{3}[Pt(d)$\rightarrow$Pb(sp)] with some metal-mediated intraligand ($^3\pi\pi$/^{3}ILCT) contribution. In contrast to **1** and **2**, **3** does not show vapoluminescent behaviour.

Introduction

The study of intermetallic interactions between closed shell metals is a field of continuous interest in Inorganic and Organometallic Chemistry.[1-11] The appeal of these interactions resides not only in their use as a powerful tool in the design of interesting supramolecular architectures,[12-30] but also in their intriguing photophysical and photochemical properties.[17,31-43]

Interestingly, some of these heterometallic systems with metal-metal bonds were found to show reversible color and emission changes in response to external stimuli as volatile organic compounds (VOCs) (vapochromic/vapoluminescence) or mechanical force (mechanochromism), with extensive applications as photofunctional materials. This behaviour generally originates from molecular changes in the solid state caused by modification of metal-metal contacts, coordination or crystal inclusion of VOCs or alteration of weak non-covalent interactions ($\pi\cdots\pi$ interactions, hydrogen bonding, C-H$\cdots\pi$ interactions).[44-48]

Within this area, a great number of systems stabilized by donor-acceptor Pt→M' bonds have been reported.[12-17,21-24,26,27,30,49-65] Among the acceptors M', configuration d^{10} is the most widely represented, specially Ag(I) and, to a much lesser extent, Au(I), Hg(II) and Cd(II). In contrast to these Pt(d^8)→M'(d^{10}) systems, heteropolynuclear Pt(d^8)→M'($d^{10}s^2$) (M' = Tl(I), Pb(II)) derivatives have been comparatively much less explored. With regard to Pt(II)→Tl(I) heteropolynuclear clusters, several structural configurations have been reported, including di (PtTl),[21,50,66-68] tri ($PtTl_2$,[69-72] Pt_2Tl,[16,56,73,74]), tetra ("paired" $(PtTl)_2$,[21,54,75-78] trigonal Pt_3Tl[29,79]), hexanuclear clusters (Pt_2Tl_4,[78,80] Pt_3Tl_3[79]), or even infinite networks.[16,74,76,78,80,81] In comparison, the number of polymetallic complexes containing Pt(II)→Pb(II) bonds is much more scarce,[17,24,48,67,82-87] and little is known about their luminescent properties.[17,24,85] One point of interest in these systems is the stereoactivity of the $6s^2$ electron pair of the heavy ion, particularly relevant in Pb(II) systems,[88-92] which exerts a notable influence in their structures, categorized as *hemi-* or *holodirected*. Mixing of 6s and 6p orbitals leads to a stereochemically active lone pair, generating *hemidirected* structures with a void in the coordination sphere of the Pb(II) and lower coordination numbers, whereas symmetrical *holodirected* environments are usually found with high coordination numbers. It is now stablished that different degrees of activity of the lone pair produce

subtle modifications of the structure and in their photophysical responses to external stimuli.[48,86,87] In spite of this, so far only a few Pt(II)–Tl(I)/Pb(II) systems form dynamic stimuli responsive materials.[80,86,48,87]

In the course of our recent research, we have developed synthetic methods for the preparation of complexes containing Pt(II)→M donor-acceptor bonds, using as platinum starting materials complexes containing the cyclometalated ligand 7,8 benzoquinolinyl (bzq).[13,14,21,27,30,48,65,93] In particular, the anionic $[Pt(bzq)(C_6F_5)_2]^-$ fragment has allowed us to form a rare bimetallic cationic complex $[\{Pt(bzq)(C_6F_5)_2\}Cd(cyclen)]^+$ (cyclen = 1,4,7,10-tetraazacyclododecane), exclusively stabilized by a Pt→Cd bond,[14] and several bi- and trinuclear Pt-Ag complexes featuring synergistic Pt→Ag bonds[13,27,30,48,65] and η^1-C_{bzq}-Ag bonding interactions and supramolecular π···π interactions between the aromatic rings of the bzq ligand.

In this paper we expand our study on the ability of the synthon $[Pt(bzq)(C_6F_5)_2]^-$ to act as a precursor in the formation of complexes containing Pt→M bonds. We report here the preparation, structural characterization and optical properties of one unexpected infinite helicoidal chain $[\{Pt(bzq)(C_6F_5)_2\}Tl(Me_2CO)]_n$ **1** and two trinuclear Pt_2M clusters $[\{Pt(bzq)(C_6F_5)_2\}_2M]^n$ (n = -1, M = Tl **2**; n = 0, M = Pb **3**), stabilized by Pt(II)→Tl(I)/Pb(II) dative bonds. The Tl(I) chain **1** displays reversible vapochromic and vapoluminescent responses to small donor solvents (THF and Et_2O), likely related to the sorption/desorption of donor molecules, which modify the guest molecule coordinated to the Tl(I) ion. It also shows mechanochromic behaviour, which is associated to variation of the intermetallic Pt(II)–Tl(I) separation in the chain caused by grinding. The trinuclear Pt_2Tl compound **2** shows smaller vapoluminescent behaviour and slower desolvation process in comparison to **1**, whereas the Pt_2Pb compound **3** does not show response to external stimuli.

Results and discussion

Synthesis and Structural Characterization

Complexes with Pt→Tl bonds. As shown in Scheme 1, the reactions of $(NBu_4)[Pt(bzq)(C_6F_5)_2]$ (**A**) with $TlPF_6$ in acetone render the neutral extended chain $[\{Pt(bzq)(C_6F_5)_2\}Tl(Me_2CO)]_n$ (**1**) or the discrete trimetallic anionic complex $(NBu_4)[\{Pt(bzq)(C_6F_5)_2\}_2Tl]$ (**2**), depending on the molar ratio of the reactions.

The crystal structure of **1** (Figure 1, Tables 1 and S1) confirms that **1** forms an infinite ···Pt–Tl–Pt–Tl··· chain with alternate "Pt(bzq)$(C_6F_5)_2$" and "Tl" fragments, which is maintained by Pt→Tl bonds. As far as we know, there is only another example of a one-dimensional (1D) heterometallic linear chain stabilized only by Pt(II)–Tl(I) bonds, without conventional bridging ligands, namely complex $(NBu_4)_n[\{Pt(C_6F_5)_4\}Tl]_n$.[16] In **1**, the Pt–Tl distances [2.961(1)-3.067(1) Å] are similar to those found in $(NBu_4)_n[\{Pt(C_6F_5)_4\}Tl]_n$, and in the usual range described for other Pt(II)–Tl(I) complexes with no bridging ligands between the atom centres.[29,68,70,71,74-77,79-81,94] The Pt-Tl vectors are near perpendicular to the square planar basal plane [angles 12.0(1)º and 16.4(1)º]. Each Tl centre is relatively near from four *ortho*-fluorine atoms, with $Tl^{\cdots}F_o$ distances [range 3.027(3)-3.083(4) Å] noticeably lower than the sum of the van der Waals radii of Tl and F (3.43 Å),[95] thus probably contributing to the final stabilisation of the chain.[16,76] The environment of the Tl centres is completed by a weak interaction with the oxygen atom of an acetone molecule [Tl(1)–O(1) 2.805(6) Å, Tl(2)–O(2) 2.720(5) Å],[76,80,94,96] located between consecutive bzq planes. The existence of these Tl–O interactions seems not to affect the strength of the Pt–Tl bonds, since the intermetallic distances are comparable to that reported in the related complex $(NBu_4)_n[\{Pt(C_6F_5)_4\}Tl]_n$.[16] In contrast to the linear –[Tl-Pt]– sequence observed in this homoleptic chain, in **1** the ···Pt–Tl–Pt–Tl··· sequence is not linear [Tl(1)–Pt(1)–Tl(2) 159.81(1)º, Tl(1)–Pt(2)–Tl(2) 149.09(1)º, Pt(1)–Tl(1)–Pt(2) 154.93(1)º, Pt(1)–Tl(2)–Pt(2) 150.18(1)º]. The dihedral angles between consecutive square planes are 20.3(2)º and 17.7(2)º, respectively. The overall disposition of the molecular chain constitutes an helix, with the ligands around the Pt in the "Pt(bzq)$(C_6F_5)_2$" sub-units rotated about 90º with respect to their position in the previous sub-unit. Since the ···Pt–Tl–Pt–Tl··· wire lies essentially in a 2_1 crystallographic axis and that the asymmetric unit contains a Pt_2Tl_2 fragment, one cycle of the helix is completed every four "Pt(bzq)$(C_6F_5)_2$" fragments, being the length of the "$(\{Pt(bzq)(C_6F_5)_2\}Tl(Me_2CO))_4$" motive of 22.98 Å. An helical motive is also found in $[\{Tl[Tl\{cis\text{-}Pt(C_6F_5)_2(CN)_2\}]_n$[76] and in the related complex $[\{Pt(bzq)(C_6F_5)_2\}Ag]_n$, with a span of 14.13 Å.[27]

As an additional note, it is noteworthy to mention that one of the bzq ligands present in a asymmetric unit is disordered over two positions with a partial occupancy 0.7/0.3, in such a way that the position of the nitrogen atom is inverted with respect to the other disordered representation. This disorder does not affect the essential

parameters of the polymeric structure, since the rings of the two disordered dispositions of the bzq ligands are almost superimposable, and the structural data given in this text refer to the majority component of the disorder.

Complex **2** has been crystallised in three different forms (Figures 2 and S1, Tables 1 and S2): two indistinguishable pseudo-polymorphs[97] **2**·0.75CH_2Cl_2 (**2a**) and **2**·CH_2Cl_2 (**2b**), obtained by crystallization from CH_2Cl_2/*n*-hexane and the adduct **2**·THF (**2c**), obtained by crystallization from THF/*n*-hexane. The measured optical properties (absorption and emission, see below) are of the bulk material. In the three forms, the anions present a "sandwich" type structure with a Tl(I) centre bonded to two "Pt(bzq)$(C_6F_5)_2$" fragments. However, in the form **2**·THF (**2c**) the molecule of THF is also coordinated to the Tl center [2.630(4) Å],[98-100] what is reflected in the bonding interactions with the platinum fragments. Thus, the two formed Pt→Tl bonds exhibit intermetallic distances slightly shorter in **2a** and **2b** than in **2c** [2.943(1), 2.881(1) Å **2a**, 2.925(1), 2.875(1) Å **2b** *vs* 2.935(1), 2.971(1) Å **2c**]. Similarly, the Pt–Tl–Pt bond sequence is not linear, being the angle at the thallium centre slightly larger in the adduct **2c** [155.91(1)º] than in **2a** and **2b** [150.65(2)º **2a**, 146.91(1)º **2b**]. As in **1**, all three forms of **2** exhibit four relatively short *o*-F···Tl distances [2.900(6)-3.150(4) Å **2a**; 2.850(4)-3.200(3) Å **2b**; 3.106(3)-3.255(3) Å **2c**], that might indicate the existence of weak additional stabilising contacts. These contacts are slightly weaker for **2c**, probably due to the extra contribution of the THF to the electronic requirements of the acidic Tl center.

A noteworthy difference between the two forms (**2a**, **2b**) crystallized from CH_2Cl_2/*n*-hexane is the different disposition of the two Pt(bzq) units. While in **2b** they adopt a relative *syn* disposition, in **2a** (and also in **2c**) the two Pt(bzq) units are *anti* each other (See Figure S1). A similar situation was found in the related complexes $[\{Pt(bzq)(C_6F_5)_2\}_2Ag]^-$,[13] $[\{Pt(bzq)(C_6F_5)L\}_2Ag]$,[30,65] and in the minor component of the disorder found in the structure of **1**. There are also differences in the supramolecular arrangement of the $[\{Pt(bzq)(C_6F_5)_2\}_2Tl]^-$ anions. Thus, while for **2b** the bzq ligands of two neighbour anion complexes stack with an interplanar distance of *ca.* 3.6 Å, establishing weak π···π interactions and forming dimers in a similar way to other "Pt(bzq)" complexes (See Figure S1c),[13,14,17,30,65,101-106] neither **2a** nor **2c** show these interactions. This is due to the fact that the NBu_4^+ cations locate just in front of the external face of the bzq ligands preventing other anion to come close.

Complexes **1** and **2** were fully characterized by analytical and spectroscopic techniques and their integrity in solution was studied by multinuclear (^{1}H, ^{19}F (CD_3COCD_3, CD_2Cl_2) and ^{195}Pt{^{1}H}) NMR spectroscopy. The MALDI(+) mass spectrum of **1**, using DCTB in acetone as matrix, gave the fragmentation peaks corresponding to the Pt-Tl fragments $[Pt(bzq)(C_6F_5)_2Tl(CH_3COCH_3)]^+$ (*m/z* 957, 40%) and $[Pt(bzq)(C_6F_5)_2Tl_2]^+$ (*m/z* 1116, 12%). In its MALDI(-) spectrum appear the peaks corresponding to $[Pt(bzq)(C_6F_5)_2]^-$ (*m/z* 707) and $[\{Pt(bzq)(C_6F_5)_2\}_2Tl]^-$ (*m/z* 1620). The MALDI spectra for **2** show in (+) mode the Pt-Tl fragments $[Pt(bzq)Tl(CH_3COCH_3)]^+$ (*m/z* 623) and $[Pt(bzq)(C_6F_5)_2Tl(CH_3COCH_3)]^+$ (*m/z* 957), whereas in (-) mode the peak associated to $[Pt(bzq)(C_6F_5)_2]^-$ (*m/z* 707). These spectra might suggest a fragmentation of the complexes in solution via partial rupturing of Pt···Tl bonding interactions. Indeed, the molar conductivity in acetone gives a value of 48 $\Omega^{-1}cm^{-2}mol^{-1}$ for **1**, in accordance with a partial dissociation of the Pt-Tl bond, and 118 $\Omega^{-1}cm^{-2}mol^{-1}$ for **2**, corresponding to a 1:1 electrolyte.

Additional, relevant information was obtained from ^{19}F NMR spectroscopy. Thus, in CD_3COCD_3, complex **1** exhibits signals compatible with the existence of two AA'MM'X spin systems, in accordance with the inequivalence of the two C_6F_5 ligands on the platinum fragments. The *ortho*-fluorine resonances are seen down (by 0.5 ppm, C_6F_5 *trans* to C) and up (by 1.6 ppm, C_6F_5 *trans* to N) shifted, respectively, in comparison to the precursor, thus supporting the presence of fragments having Pt-Tl bonds in solution. Significantly, the ^{195}Pt-*o*-F coupling constants are notably smaller than those in the starting precursor (223 and 426 Hz **1** *vs* 310 and 580 Hz **A**), what is consistent with the increase in the coordination number upon formation of Pt-Tl bonds. At low temperature (198 K), both *o*-fluorine signals broaden, indicating a dynamic behaviour. The ^{195}Pt{^{1}H} NMR spectrum (CD_3COCD_3) shows a singlet notably deshielded in relation to the precursor (-2826 **1** *vs* -3705 ppm **A**), further supporting the presence of Pt-Tl bonds in solution. In addition, the lack of an observable coupling between Pt and Tl atoms also suggests that the Pt-Tl bond is dynamic on the NMR time scale. Addition of successive amounts of $TlPF_6$ to a solution of complex **1** at room temperature, only causes a negligible reduction of the $^{3}J_{o\text{-F-Pt}}$ coupling constants (from 223, 420 to 219, 415 Hz, Figure S2), whereas addition of successive amounts of starting material $(NBu_4)[Pt(bzq)(C_6F_5)_2]$ (**A**) produces a displacement of the *o*-F signals with a concomitant increase of the $^{3}J_{o\text{-F-Pt}}$ coupling constants (Figure S3). When 1 equiv. of **A** is added, **2** is formed (Scheme 2i), but not signals for pure **A** are observed. These

spectra are consistent with the equilibria shown in Scheme 2. It is suggested that dissolution of the chain **1** in acetone mainly occurs as solvated bimetallic [Pt(bzq)(C_6F_5)$_2$Tl(S_x)] fragments, which are additionally involved, in low extent, in a fast equilibrium with the anionic precursor *via* cleavage of the Pt-Tl bond (Scheme 2ii). The ^{19}F NMR spectra of **1** in CD_2Cl_2 reveal a more rigid behaviour (see Figure S4). At room temperature, the *para* and *meta* (broad) fluorine resonances are observed, whereas the *ortho*-F do not raise from the baseline, indicative of dynamic behaviour. Unfortunately, its low solubility prevented to obtain good NMR spectra at low temperature in this solvent.

For complex **2**, we observed that the data (δ and $^3J_{o\text{-F-Pt}}$) obtained of their ^{19}F NMR spectra in CD_3COCD_3 depend on the concentration, what is also consistent with a dynamic behaviour. As is shown in Figure S5, dilution of a solution from 8.9×10^{-3} M to 1×10^{-4} M causes a progressive shift of the signals of the F_{ortho} and a concomitant increase of the $^3J_{o\text{-F-Pt}}$ (from 250 to 265 Hz and 480 to 510 Hz; Data given for 1×10^{-3} M in the Experimental Section). In any case, the $^3J_{o\text{-F-Pt}}$ coupling constants are smaller than in **A**, confirming the presence of Pt-Tl bonds in solution (also supported by the ^{195}Pt{^{1}H} NMR, -3052 **2** *vs* -3705 ppm **A**). At low temperature (198 K), only broadening of the two *o*-fluorine signals was observed. When successive amounts of **A** are added to a solution of **2**, a displacement of the signals toward those observed for **A** takes place, thus confirming the occurrence of a fast equilibrium between **2**, **A** and Tl^+ (Scheme 2iii), which averages the chemical shifts corresponding to **2** and **A** (Figure S6). In a same way than for **1**, the coupling constants increase with the additional incorporation of **A** in solution. The ^{19}F NMR spectra of **2** were also recorded in CD_2Cl_2, revealing a more rigid behaviour than in acetone (broader signals) and persistence of Tl···F contacts in solution (Figure S7). At 298 K, **2** shows two sets of AA'MXX' patterns (as in acetone). When the temperature is lowered, the *o*-F broaden and coalesce at 238 K and at 198 K a rigid pattern for a trinuclear species with the Tl(I) interacting with four non-equivalent *o*-fluorine atoms is observed. A very broad resonance appears at δ -117.1 ppm, due to the *o*-F *exo* atoms, whereas the *o*-F *endo* give rise to four extensive doublets due to the short contacts ^{203,205}Tl···F. Unfortunately, the corresponding coupling constants cannot be calculated, because only the external signals of the doublets are clearly visible, as the internal are overlapped with the *exo*-F signal.

Complexes with Pt→Pb bonds. As said above, in comparison with Tl, the reports of complexes containing Pt(II)→Pb(II) dative bonds are scarce.[17,24,48,83,85,86] As it was noted by Balch *et al.* some years ago,[82] Pb(II) seems to be much less prone to establish this kind of interactions than Tl(I). However, complex $(NBu_4)[Pt(bzq)(C_6F_5)_2]$ (**A**) seems to be an adequate precursor for the preparation of polynuclear complexes with Pt→Pb donor acceptor bonds. Indeed, the reaction of **A** with $PbClO_4.3H_2O$ in 2:1 molar ratio in acetone renders, after workup of the resulting solution, the complex $[\{Pt(bzq)(C_6F_5)_2\}_2Pb]$ (**3**) as an yellow-orange solid. The crystal structure of this complex determined by X-ray diffraction is shown in Figure 3. Tables 1 and S3 lists its more relevant bond lengths and angles. As can be seen, **3** is a trinuclear type "sandwich" complex very similar to $[\{Pt(bzq)(C_6F_5)_2\}_2Ag]^-$ [13] or $[\{Pt(bzq)(C_6F_5)_2\}_2Tl]^-$ (**2**). The complex contains two Pt→Pb bonds unsupported by any conventional bridging ligand, the Pt–Pb distances being 2.776(1) Å, in the range found for the similar Pt–Pb complexes mentioned above.[17,24,83,85,86] This distance is shorter than those found in the forms of **2** $[\{Pt(bzq)(C_6F_5)_2\}_2Tl]^-$ [**2a**-**2c**, range from 2.875(1) Å to 2.973(1) Å, *vide supra*], and a similar trend has been previously observed in the isolectronic homoleptic anions $[\{Pt(C_6F_5)_4\}_2Tl]^{3-}$ [Pt–Tl 2.978(1), 3.043(1) Å][16]/ $[\{Pt(C_6F_5)_4\}_2Pb]^{2-}$ [Pt–Pb 2.769(2), 2.793(2) Å].[83] This structural feature can be attributed to the smaller size of the ion Pb(II) in relation to Tl(I),[107] taking into account that these systems usually display a notable electrostatic contribution to the M-M' bonding interactions.[108] The Pt–Pb–Pt angle is 150.26(2)º, similar to the isostructural Tl(I) forms of **2** [146.91(1)-155.9(1)º], leading to a void in the opposite hemisphere, indicative of some steroactivity of the $6s^2$ lone pair on the M. The formation of bent Pt-M-Pt units contrasts with the almost linear arrangement displayed by the homoleptic anions $[\{Pt(C_6F_5)_4\}_2Tl]^{3-}$ [Pt–Tl–Pt 174.01(2)º][16] and $[\{Pt(C_6F_5)_4\}_2Pb]^{2-}$ [Pt–Pb–Pt 178.6(1)º],[83] respectively. In these latter, the Pb(II) or Tl(I) ion achieves an *holodirected* bicapped antiprismatic environment with additional eight *o*-F contacts (four of each Pt fragments). By contrast, in **3** (and also in **2**), the lower charge on the platinum atoms and the planarity of the aromatic ancillary bzq ligand in the platinum units seem to play a key role in the final *hemidirected* coordination at the M (Pb(II) or Tl(I)) ions. Indeed, as in **2**, the environment of the Pb centre in **3** is supplemented by secondary contacts with the four *endo ortho* fluorine atoms of C_6F_5 ligands [2.972(4) Å F(1), 2.792(5) Å F(6)]. The shorter *o*-F···Pb distances in **3** with respect to those *o*-F···Tl in the analogous forms of **2** are in accordance with the smaller intermetallic Pt-Pb separation.

The [{Pt(bzq)(C_6F_5)$_2$}$_2$Pb] units arrange in the crystal structure in such a way that the bzq plane is parallel to the bzq plane of a neighbouring anion, resulting in an infinite stacking of anions related by π-π interactions (~ 3.4 Å, see Figure 3b), contrasting with the stacking in pairs found in the anions **2b** and **2c**.

The MALDI(+) mass spectrum of **3** shows the peak corresponding to the fragment $[Pt_2(bzq)_2(C_6F_5)_3Pb]^+$ (*m/z* 1454), together with the peak corresponding to $[Pt(bzq)(C_6F_5)_2Pb]^+$ (*m/z* 913). In agreement, the molar conductivity measurements in acetone for this neutral derivative give a value of 35 $\Omega^{-1}cm^{-2}mol^{-1}$, suggesting some degree of dissociation via breaking of Pt···Pb bonding interactions. The ^{1}H NMR spectrum of **3** shows signals for only one type of bzq ligand, while the ^{19}F NMR spectrum in CD_3COCD_3 at 298 K shows two types of C_6F_5 groups, with typical AA'MM'X spin systems, indicating that the Pt coordination is a symmetry plane in the NMR time scale. As in the previous complexes, the equivalence of the two *o*-F of the same group can take place by rotation of the C_6F_5 ligands around the Pt–C_{ipso} bonds or by cleavage and re-formation of the Pt–Pb bonds. In any case, the low solubility of **3** in acetone-*d6* (or CD_2Cl_2) prevents further studies of the ^{19}F NMR spectra at variable temperature.

Photophysical Properties

Absorption Spectra. UV-vis spectra data in solution and in solid state (diffuse reflectance) of complexes **1-3** and the previously published starting material **A** are summarized in Table 2. The analysis of the absorption profile of the extended PtTl complex **1** dissolved in THF and in CH_2Cl_2 points that the extended chain dissolves probably as bimetallic fragments [{Pt(bzq)(C_6F_5)$_2$}TlS$_n$] (S = solvent) with donor solvent molecules coordinated to the thallium centre, which is also suggested by NMR spectroscopy and mass spectrometry (see above). It shows high energy ^{1}IL absorptions (range 240-373 nm) and a less intense band (415 nm THF, 410 nm CH_2Cl_2) ascribed, with reference to previous spectroscopic work and theoretical calculations in related binuclear complexes [{Pt(bzq)(C_6F_5)$_2$}Ag(L)] (L = PPh_3, tht)[13,27] and in the extended chain [{Pt(bzq)(C_6F_5)$_2$}Ag]$_n$,[27] to an admixture of metal-to-ligand ^{1}[5d_π(Pt)→π*(bzq)] and ligand to ligand ^{1}[(C_6F_5)→bzq] charge transfer transitions (Figure 4). This low-energy band is blue-shifted in relation to the precursor **A** in THF (415 **1** *vs* 448 nm **A**) and in CH_2Cl_2 (410 **1** *vs* 425 nm **A**). This fact is consistent with the predominance of

bimetallic fragments with a Pt-Tl donor-acceptor bond, which increases the electrophilicity of the Pt centre and lower the energy of the HOMO, resulting in an increase of the energy gap of the ^{1}MLCT ^{1}[Pt(d)→π*(bzq)] transition.

The absorption spectra of the trinuclear complexes **2** and **3** in THF solutions also exhibit a blue-shift in the low-energy absorption maxima in relation to **A** (406 **2**, 416 **3** *vs* 448 nm **A**, THF) (Figure 4), whereas in CH_2Cl_2 they show a notable red-shift, more marked in the Pt_2Pb derivative (430 **2**, 440, 511 **3** *vs* 425 nm **A**, CH_2Cl_2) (Figure S8). The different behaviour of **2** and **3** in both solvents could be associated to a more extensive cleavage of the Pt-M (M = Tl, Pb) bonds in THF solution than in CH_2Cl_2 solution in which the trinuclear entities could be predominant. For complex **2**, this fact is supported by the NMR spectroscopy at variable temperature (see above, Figure S7), whereas for **3,** which is more insoluble, is also suggested by mass spectrometry and by the similarity between the absorption spectra in CH_2Cl_2 and in the solid state (diffuse reflectance, Figure S9). Probably, the presence of two Pt-M bonds in the trinuclear entity decreases the contribution from the bzq ligand and increases the metallic character (Pt/M) of both the HOMO and the LUMO orbitals with respect to those of the starting material. The change in the frontier orbitals modifies the nature of the low lying absorptions from a typical ^{1}MLCT in THF to a metal-metal charge transfer (^{1}MM'CT) in CH_2Cl_2, which is consistent with the observed red-shift. The effect of the increasing of the metallic character (Pt/Ag) in the FOs in the trinuclear Pt_2Ag derivatives [{Pt(bzq)(C_6F_5)L}$_2$Ag]ClO_4 (L = tht, MeCN, CN^{t}Bu, CN-Np) in relation to the binuclear PtAg derivatives [{Pt(bzq)(C_6F_5)L}AgL']ClO_4 (L = PPh_3, L' = $pyPh_2$; L = CN^{t}Bu, CN-2,6-Me_2Ph, L' = PPh_3) has been recently confirmed by TD-DFT calculations.[30,65]

The solid state diffuse reflectance spectrum of the extended chain **1** exhibits a characteristic low-energy feature (500-600 nm) (Figure S9), which is clearly absent in the precursor and in the trinuclear derivatives **2** and **3**. This feature is tentatively assigned, as in the extended chain [{Pt(bzq)(C_6F_5)$_2$}Ag]$_n$,[27] to an admixture of ^{1}LMM'CT ^{1}[Pt(bzq)→Tl] and ^{1}L'M'CT ^{1}[(C_6F_5)→Tl], involving the promotion of electron density from platinum "Pt(bzq)(C_6F_5)" fragments to the thallium centre. For complexes **2** and **3**, the spectra are similar to those in CH_2Cl_2 solution, suggesting that the π····π intermolecular interactions observed in the solid state have a very small effect, if any, in the lowest-energy absorption maxima. The feature in the region 430-540 nm is

greatly enhanced in comparison to the precursor **A**, which correlates well with the existence of two Pt-M (M = Tl, Pb) bonds.

Emission spectra. All complexes are brightly emissive in the solid state (Table 3), in glassy solutions and in degassed CH_2Cl_2 solutions at 298 K (Table S4), except **3**, for which no emission is detected in solution at room temperature (see below).

Solid state. The extended [-Pt-Tl-Pt-Tl-] chain **1** exhibits in the solid state at 298 K a bright (ϕ = 28.4 %) orange-red phosphorescent emission (610 nm), which is significantly red-shifted when cool down to 77 K (685 nm), pointing to the important metallic (Pt, Tl) contribution from the Pt-Tl bonds to the frontier orbitals (^{3}MM'CT) (Figure 5). This behaviour is consistent with a decrease in the Pt-Tl separation caused by thermal contraction, a phenomenon that has many precedents in extended metal···metal chain systems.[109,110] At 298 K, the emission decay was best fitted to two components [0.2 (66%), 0.6 μs (34%)], which might be attributed to small different arrangements,[48] as evidenced in its X-ray diffraction analysis. The lifetime increases remarkably at 77 K (10 μs), a feature generally attributed to the suppression of thermally activated nonradiative process. By comparison, the homoleptic $(NBu_4)_n[\{Pt(C_6F_5)_4\}Tl]_n$ displays a blue shifted emission, both at 298 (582 nm, τ = 11.6 μs) and at 77 K (635 nm, τ = 12.6 μs).[16]

At room temperature, the emission profile of the as-obtained solid trinuclear Pt_2Tl derivative **2** is similar to that of the extended chain **1** with its maximum barely shifted to lower energies (λ_{max} 615 nm). Despite the presence of pseudopolymorphs in the crystals (see above), the emission decay of the crude solid fits to one component of 1.5 μs and the measured quantum yield (ϕ = 31.7 %) is slightly higher than in **1**. At 77 K, the emission clearly resolves into two bands: a weak high-energy (HE) feature (λ_{max} 512 nm) and an intense, symmetrical low-energy (LE) band (λ_{max} 640 nm), with its maximum red-shifted with respect to that at 298 K (Figure S10). The HE structured emission with a long lifetime of 41.1 μs, is assigned to typical ^{3}IL/^{3}MLCT emission from the platinum fragments, whereas the LE band with shorter lifetime (11 μs) is ascribed to excited state with strong metallic contribution. The emission in **2** is notably red-shifted in relation to those of the related trinuclear derivatives $(NBu_4)_3[\{Pt(C_6F_5)_4\}_2Tl]$ (450 nm, 298 K; 445 nm, 77 K)[16] and $[Tl_2Pt(CN)_4]$ (448 nm),[69] which have been attributed to a metal-centred phosphorescence process

[Pt(5dz^2)→Tl(6p$_z$)] (^{3}MM'CT), within the trinuclear entity. The observed shift in **2** might be attributed to the presence of slightly stronger Pt-Tl bonds, as deduced by comparing intermetallic distances (2.8747(3)-2.9705(6) Å [{Pt(bzq)(C$_6$F$_5$)$_2$}$_2$Tl]$^-$ *vs* 2.9777(4), 3.0434(4) Å [{Pt(C$_6$F$_5$)$_4$}$_2$Tl]$^{3-}$, 3.140(1) Å [Tl$_2$Pt(CN)$_4$]), and mainly to the contribution of the planar and low lying cyclometalated bzq ligand to the frontier orbitals, which likely reduces the gap of the transition. The emission is tentatively ascribed to charge transfer from the platinum fragments to the thallium [^{3}(L+L')MM'CT].

Despite that the Pt-Pb bond distance in **3** is shorter than those of Pt-Tl in **2**, the emission of complex Pt$_2$Pb **3** in solid state at 298 K appears blue-shifted (λ_{max} = 547 nm, ϕ = 20 %) in relation to **2**. The energy maximum remains essentially unchanged at 77 K (Figure S11), but the measured lifetime increases significantly (61.7 μs) in relation to 298 K [0.02(44%), 0.5 (56.1%) μs], pointing to a higher degree of intraligand contribution. This emission can be compared to that observed in the trinuclear complex (NBu$_4$)$_2$[{Pt(C$_6$F$_5$)$_4$}$_2$Pb] (539 nm, τ = 9 μs, 298 K; 529 nm, τ = 35 μs, 77 K),[17] which was attributed to phosphorescence of the ^{3}(dσ*pσ) excited state, related to the linear trinuclear Pt-Pb-Pt entity. Considering this result and also previous works on heteropolynuclear bzq/C$_6$F$_5$ Pt^{II}-Pb complexes,[17,48,87] the emission in **3** is tentatively ascribed to metal centred charge transfer ^{3}MM'CT ^{3}[Pt(d)→Pb(sp)] mixed with metal-mediated intraligand (^{3}ππ/^{3}ILCT) contribution, as supported by the relatively long lifetime and the chain packing observed in the crystal structure (Figure 3b).

Vapochromic, Vapoluminescent and Mechanochromic Properties. The as-obtained orange-red powder **1** shows the same color and luminescence as in the crystalline form [{Pt(bzq)(C$_6$F$_5$)$_2$}Tl(CH$_3$COCH$_3$)]$_n$. Addition of a drop of MeOH or MeCN has no visual effect in the color or the emission, whereas addition of CH$_2$Cl$_2$ provokes a very quick change to yellow but an immediate recovering of the initial orange colour. However, the treatment of powder **1** with a drop of THF or Et$_2$O (fresh **1-THF** and **1-Et$_2$O** solvates) causes color and luminescence changes that can be studied. Thus, when **1** was treated with a drop of THF, a color change occurred from orange-red to yellow under ambient light and the bright orange-red luminescence turned to yellow under UV-light (Figure 6). This behaviour is reflected in a blue-shift in the emission spectra both, at 298 K (610→560 nm, ϕ = 19.3 %) and at 77 K (685→618 nm). The solid **1** and the fresh solvates **1-THF** and **1-Et$_2$O** display different excitation spectra, giving rise to

similar Stokes shifts (~2250 **1**, 1985 **1-THF**, 2100 cm^{-1} **1-Et_2O**). On standing under ambient conditions, the THF is gradually lost (1h, 580 nm 298 K; 630 nm 77 K, Figure S12), showing the sample an emission at 600 nm after 12 h. A fresh **1-Et_2O**-solvate (Figure S13) also shows color change to yellow and a significant blue-shift of the emission to 577 nm at room temperature (617 nm, 77 K). On standing, the diethyl-ether is also lost, recovering the sample its initial orange-red color (1 h, 605 nm, 298 K, 660 nm 77 K; 12 h, 617 nm, 298 K, 680 nm 77 K). Similar response in color and in luminescence were observed when solid **1** was exposed to THF and Et_2O vapors at 298 K, indicating that the transformation to **1-THF** or **1-Et_2O** adducts has occurred. After exposure of solid **1** for 30 min to THF vapors, the color and the emission change (λ_{max} 560 nm), whereas **1** exposed to diethyl-ether vapor requires only 10 min to change the solid state colour and luminescence (λ_{max} = 577 nm). In this case, the emission efficiency is notably enhanced (ϕ = 44.4 %) in relation to the pristine solid **1**, what is associated to a remarkable reduction in the non-radiative constants (Table 3).

Desolvation by passing of a stream of acetone or air onto the adduct samples showed the reversibility of this behaviour. Upon exposure of **1-THF** to air for 5 min produces change of color and emission (from 560 to 600 nm), keeping the same emission spectra after 20 min. By passing of a stream of acetone, the luminescence changes to 580 nm in 1 min and to 610 nm in 20 min, recovering the **1-acetone** solvate, being the limit of change. The same desolvation process of **1-Et_2O** adduct requires ~10 min, both in air (λ_{max} ~ 600 nm) and in acetone vapour (λ_{max} = 610 nm). It is reasonable to conclude that the oxygen donor solvents similar to acetone (THF, Et_2O) are able to contact the Tl^I center in a way similar to that described for $[\{Pt(bzq)(C_6F_5)_2\}Tl(CH_3COCH_3)]_n$ **1**, which explains the different color and emission observed. We also found that this extended chain exhibited a notable mechanochromic behaviour. Thus, after the orange solid was ground, the resulting red powder showed a red shift in its emission spectra (λ_{max} 665 nm 298 K, 685 nm 77 K) with a remarkable decreases in its quantum yield (ϕ = 2.4%). The notable red shift in the crushed powder at room temperature suggests a shortening in the metal-metal separation in the chain caused by grinding.

We have also observed that the as-obtained solid **2** (precipitated in acetone) shows small changes (from 615 to 595 acetone, 590 THF, 588 Et_2O) in the emission maxima upon treatment with a drop of the corresponding donor solvent or vapours (~ 10 min, acetone; ~ 15 min, THF; ~1h Et_2O) (see Figure 7 and Table 3). The emission of **2** upon

treatment with THF vapours coincides with that of crystals of the adduct **2·THF** (see X-ray). The measured lifetimes of the likely formed solvates are in the same range than **2**, but the emission efficiencies decrease, particularly for **2-THF** (0.4 % **2-THF**, 20.1 % **2-Et_2O**, 30.3 % **2-Me_2CO** *vs* 31.7 % **2**) for which both the K_r and K_{nr} decreases and increases one order of magnitude, respectively. The desolvation process, when passing a stream of air onto the samples **2-Me_2CO**, **2-THF** or **2-Et_2O**, monitored using emission spectroscopy, showed that the process is slow, precluding its possible use as a sensor.

In contrast with the behaviour commented, the changes in the color and in the emission colour of **3** by treatment of a drop or exposure to vapours of donor solvents such as MeCN, THF or Et_2O are negligible. We neither observed color or significant emission changes by crushing the solid in a ceramic mortar.

Solution. Although **1** is not good emitter in solutions at 298 K, it becomes brightly emissive at 77 K (see Table S4). In glassy solutions (77 K), the color and the emissions are dependent on the solvent, concentration and excitation wavelength, exhibiting thermochromism. In concentrated THF solutions (10^{-3} M, deep orange glasses), **1** displays a broad low-energy emission band (600 nm). However, upon dilution, different bands are observed depending on the wavelength used for excitation (5×10^{-4} M, pale-orange glasses, bands in the range 485 to 640 nm; 5×10^{-5} M, white glasses, emission bands in the range 480 to 590 nm). Similar behaviour is observed in CH_2Cl_2 (purple glasses) and in acetone (orange to white glasses), giving rise the lowest energy emissions in CH_2Cl_2 (λ_{max} 690 nm). As illustration of this, the emission spectra of **1** in THF at concentrations from 10^{-3} to 5×10^{-5} M and at several excitation wavelengths are shown in Figure 8. The observed change in the colours of glasses indicates that this behaviour probably results from changes in the size of the aggregates formed (in the frozen process) and the Pt···Tl distances within the aggregates in the ground state. As it is expected, the formation of extended aggregates which emit at similar energies or even lower energies than in the solid is favoured in the most concentrated solutions and using low-energy wavelength of excitation. The structured HE emission (~ 480 nm) resembles the emission of the precursor **A** (485, 522, 565, 611_{sh} THF, 77 K; 485, 521, 563, 608_{sh} CH_2Cl_2, 77 K) being, therefore, ascribed to mixed ^{3}MLCT/^{3}LC of the platinum fragments, whereas the intermediate multiple emissions are mainly attributed to admixture of ^{3}MM'CT/^{3}ILCT excited states on multiple discrete ground (or excimeric) $[\{Pt(bzq)(C_6F_5)_2\}_2Tl]^-$ units.

The room-temperature yellow solutions of **2** in CH_2Cl_2 shows an unstructured band centred at 610 nm, similar to that observed in solid state, suggesting the integrity of the trinuclear $[Pt_2Tl]^-$ anions in solution (Figure S14). This emission band in fluid media is slightly redshifted in relation to that observed in glassy solution (λ_{max} 570 nm). The occurrence of rigidochromism in heteropolynuclear complexes has many precedents[111] and has been ascribed to the larger structural changes that are accessible in solution than in rigid media. As in the solid state, a minor high-energy feature at 487 nm is also observed in glassy media (Figure S14).

The trinuclear Pt_2Pb derivative **3** is only emissive in glassy solutions. In diluted (5×10^{-5} M) CH_2Cl_2 glass two bands with different intensity (525 minor, 570 nm major) and different excitation spectra were obtained (Figure S15). By increasing the concentration to 5×10^{-4} M, the minor band decreases, what indicate again the formation of two different ground-state observing species. It is worth to note that the major low-energy feature, attributed to emission in the trinuclear Pt_2Pb unit (^{3}MM'CT/^{3}ILCT), is notably red shifted with respect to the emission in solid at 77 K (547 nm), probably due to the occurrence of intermolecular $\pi\cdots\pi$ interactions between the chromophores Pt_2Pb.

Conclusions

In summary, we report the synthesis and structures of a Pt-Tl chain $[\{Pt(bzq)(C_6F_5)_2\}Tl(Me_2CO)]_n$ (**1**) and two novel isoelectronic trinuclear Pt_2M [M = Tl(I), Pb(II)] complexes, stabilized by donor-acceptor Pt→M bonds. NMR studies suggest the occurrence of equilibria in solution implying breaking and re-formation of Pt-M bonds. The UV-vis absorption spectra support this fact in the chain **1** in THF and CH_2Cl_2, in which bimetallic Pt-Tl fragments seem to be predominant, and in **2** and **3** in THF, exhibiting a blue-shift in the low-energy absorption band in relation to the precursor. In a less donor solvent (CH_2Cl_2) **2** and **3** show, however, a notable red-shift in the low energy absorption, which is associated to the predominance of the trinuclear units.

The Pt-Tl compounds **1** and **2** show bright orange-red emissions with very close maxima in both. This emission is mainly ascribed to platinum to thallium charge transfer (^{3}MM'CT) in **1**, with some additional contribution of the ligands [^{3}(L+L')MM´CT] (L = bzq, L' = C_6F_5) in **2**. The trinuclear Pt_2Pb complex **3** displays a yellow emission band, tentatively ascribed to admixture of ^{3}MM'CT with some metal-

mediated ^{3}ILCT contribution. **1** undergoes a bathochromic shift in color and emission upon grinding (mechanochromism), which is reversed upon fuming the sample with acetone. This behaviour is attributed to the shortening of the Pt-Tl separations in the chain induced on grinding. **1** and **2** exhibit blue-shift vapoluminescent responses to donor solvents (THF, Et_2O **1** and Me_2CO, THF, Et_2O **2**) being larger the changes and reversible the corresponding desolvation process in the neutral extended chain **1**. The crystal structures of **1**-**3** have allowed us to propose an explanation to their different behaviour towards solvent vapors. Thus, **1** having a Pt/Tl ratio 1:1, crystallizes with an acetone molecule which coordinates weakly to the Tl centre. Therefore, its vapochromic behaviour is ascribed to the fast exchange of the acetone coordinated to the Tl(I) centre by other oxygen donor solvents (THF and Et_2O). It is important to note that solid-vapor reactions involving the exchange of ligands coordinated to metal centres are quite rare.[112-115] Complex **2** forms two pseudopolymorphs in CH_2Cl_2/*n*-hexane (**2a**, **2b**) having CH_2Cl_2 molecules of solvation and the adduct **2·THF** (**2c**) with the THF molecule coordinated to the Tl(I), in THF/*n*-hexane. In this adduct, the Tl-O(THF) bonding interaction [2.630(4) Å] is notably shorter than the Tl-O(acetone) in the chain **1** [2.805(6), 2.720(5) Å], what could explain the slowness of the desolvation process observed. In contrast to the vapoluminescent behaviour of **1** and **2**, complex **3** did not show any response to liquid or vapors of donor solvents. This might be due to the smaller void space in the crystal lattice of **3** that would be unable to absorb vapour molecules. Expansion to other chromophore platinum substrates could offer a new approach to molecular materials that exhibit multistimuli responses.

Experimental

General Comments. Literature methods were used to prepare the starting material $(NBu_4)[Pt(bzq)(C_6F_5)_2]$.[14] C, H and N analyses, conductivities, IR and NMR spectra were performed as described elsewhere.[14] Mass spectra were recorded on a Microflex MALDI-TOF Bruker spectrometer operating in the linear and reflector modes using as matrix DCTB (1,1-Diciano-4-ter-butylphenyl-3-metylbutadiene) (10 mg/ml in acetone). The ratio sample/matrix used was 1/10. The optical absorption spectra were recorded using a Hewlett Packard 8453 (solution) spectrophotometer in the visible and near-UV ranges. Diffuse reflectance UV-vis (DRUV) data of pressed powder were recorded on a Shimadzu (UV-3600 spectrophotometer with a Harrick Praying Mantis accessory) and recalculated following the Kubelka-Munk function. Emission and excitation spectra

were obtained on a Perkin-Elmer Luminescence Spectrometer LS 50B and on a Jobin-Ybon Horiba Fluorolog 3-22 Tau-3 spectrofluorimeter, with the lifetime measured in phosphorimeter mode (with an F1-1029 lifetime emission PMT assembly, using a 450WXe lamp) or with a Datastation HUB-B with a nanoLED controller and software DAS6. The nanoLEDs employed for lifetime measurements were of 450 nm with pulse lengths of 0.8–1.4 ns. The lifetime data were fitted using the Jobin-Yvon software package.

Safety Note: Perchlorate salts of metal complexes with organic ligands are potentially explosive. Only small amounts of material should be prepared and these should be handled with great caution.

Synthesis of $[\{Pt(bzq)(C_6F_5)_2\}Tl(Me_2CO)]_n$ (1). To a solution of $TlPF_6$ (0.142 g, 0.408 mmol) in acetone (15 mL) $(NBu_4)[Pt(bzq)(C_6F_5)_2]$ (0.387 g, 0.408 mmol) was added. After 15 h of stirring the solution was evaporated to 2 mL and **1** crystallized. The orange-red solid was filtered off, washed with cold acetone (3 × 1 mL) and vacuum-dried, 0.188 g, 51% yield. Anal. Found (calcd for $C_{28}H_{14}F_{10}NOPtTl$): C, 34.66 (34.68); H, 1.36 (1.46); N, 1.43 (1.44). MALDI-TOF (-): *m/z* (%) 707 $[Pt(bzq)(C_6F_5)_2]^-$ (100), 1620 $[\{Pt(bzq)(C_6F_5)_2\}_2Tl]^-$ (2). MALDI-TOF (+): *m/z* (%) 957 $[Pt(bzq)(C_6F_5)_2Tl(CH_3COCH_3)]^+$ (40), 1116 $[Pt(bzq)(C_6F_5)_2Tl_2]^+$ (12). IR (cm^{-1}): 1633 (w), 1503 (s), 1060 (s), 1042 (s), 944 (s), 833 (s), 821 (s), 779 (m, C_6F_5, X-sensitive vibr.),[116] 774 (m, C_6F_5, X-sensitive vibr.),[116] 763 (s). ^{1}H NMR (Acetone-d_6, 295 K, ppm), δ 8.81 (H2, d, $^3J_{H(2),H(3)}$ = 5.1 Hz, $^3J_{H(2),Pt}$ = 28 Hz), 8.63 (H4, d, $^3J_{H(4),H(3)}$ = 7.8 Hz), 7.88 (H5, d, $^3J_{H(5),H(6)}$ = 8.7 Hz), 7.81 (H6, d, $^3J_{H(6),H(5)}$ = 9.0 Hz), 7.67 (H7, d, $^3J_{H(7),H(8)}$ = 7.8 Hz), 7.59 (H3, dd, $^3J_{H(3),H(4)}$ = 7.8 Hz, $^3J_{H(3),H(2)}$ = 5.1 Hz), 7.42 (H8, dd, $^3J_{H(8),H(7)}$ = 7.8 Hz, $^3J_{H(8),H(9)}$ = 7.2 Hz), 7.30 (H9, d, $^3J_{H(9),H(8)}$ = 7.2 Hz, $^3J_{H(9),Pt}$ = 40 Hz).^{19}F NMR (Acetone-d_6, 295 K, ppm), δ –114.6 (*o*-F, d, $^3J_{F,F}$ = 25 Hz, $^3J_{F,Pt}$ = 223 Hz), –117.5 (*o*-F, d, $^3J_{F,F}$ = 17 Hz, $^3J_{F,Pt}$ = 426 Hz), –164.8 (F, br m), –166.9 (F, br m). ^{19}F NMR (Acetone-d_6, 193 K, ppm), δ –114.4 (*o*-F, br s), –117.2 (*o*-F, br s), –163.9 (F, br m), –166.0 (F, br m). ^{195}Pt{^{1}H} NMR (Acetone-d_6, 295 K, ppm), δ –2826 (m). Λ_M (Acetone): 48 $\Omega^{-1}cm^{-2}mol^{-1}$.

Synthesis of $[NBu_4][\{Pt(bzq)(C_6F_5)_2\}_2Tl]$ (2). To a solution of $TlPF_6$ (0.070 g, 0.200 mmol) in acetone (15 mL) $(NBu_4)[Pt(bzq)(C_6F_5)_2]$ (0.380 g, 0.400 mmol) was added. After 15 h of stirring the solution was evaporated to 2 mL and **2** crystallized. The

orange solid was filtered off and washed with cold acetone (3 × 1 mL), 0.071 g, 20% yield. Anal. Found (calcd for $C_{66}H_{52}F_{20}N_3Pt_2Tl$): C, 42.97 (42.58); H, 2.70 (2.82); N, 2.14 (2.26). MALDI-TOF (-): *m/z* (%) 707 $[Pt(bzq)(C_6F_5)_2]^-$ (100). MALDI-TOF (+): *m/z* (%) 623 $[Pt(bzq)Tl(CH_3COCH_3)]^+$ (95), 957 $[Pt(bzq)(C_6F_5)_2Tl_2(CH_3COCH_3)]^+$ (100). IR (cm^{-1}): 1633 (w), 1503 (s), 1060 (s), 1042 (s), 944 (s), 833 (s), 821 (s), 779 (m, C_6F_5, X-sensitive vibr.),[116] 774 (m, C_6F_5, X-sensitive vibr.),[116] 763 (s). ^{1}H NMR (Acetone-d_6, 1 x 10^{-3} M, 298 K, ppm) δ 8.62 (H2, d, $^3J_{H(2),H(3)}$ = 3.5 Hz, $^3J_{H(2),Pt}$ = 28 Hz), 8.54 (H4, d, $^3J_{H(4),H(3)}$ = 7.7 Hz), 7.81 (H5, d, $^3J_{H(5),H(6)}$ = 8.7 Hz), 7.70 (H6, d, $^3J_{H(6),H(5)}$ = 8.5 Hz), 7.60 (H7, d, $^3J_{H(7),H(8)}$ = 7.5 Hz), 7.51 (H3, dd, $^3J_{H(3),H(4)}$ = 6.0 Hz, $^3J_{H(3),H(2)}$ = 5.1 Hz), 7.33 (H8, dd, $^3J_{H(8),H(7)}$ = 7.8 Hz, $^3J_{H(8),H(9)}$ = 6.9 Hz), 7.14 (H9, d, $^3J_{H(9),H(8)}$ = 6.5 Hz, $^3J_{H(9),Pt}$ = 42 Hz), 3.41 (8H, m, $N(C\underline{H}_2CH_2CH_2CH_3)^+$), 1.79 (8H, m, $(N(CH_2C\underline{H}_2CH_2CH_3)^+$), 1.40 (8H, sext., $(N(CH_2CH_2C\underline{H}_2CH_3)^+$), 0.96 (12H, t, $(N(CH_2CH_2CH_2C\underline{H}_3)^+$). ^{19}F NMR (Acetone-$d_6$, 1 x 10^{-3} M, 298 K, ppm), δ -114.8 (*o*-F, d, $^3J_{F,F}$ = 25 Hz, $^3J_{F,Pt}$ = 255 Hz), -116.8 (*o*-F, d, $^3J_{F,F}$ = 28 Hz, $^3J_{F,Pt}$ = 500 Hz), -165.5 (*m*-F, br m), -166.0 (*p*-F, t, $^3J_{F,F}$ = 20 Hz), -167.9 (*m*-F, br m), -168.4 (*p*-F, t, $^3J_{F,F}$ = 20 Hz). ^{19}F NMR (Acetone-d_6, 1 x 10^{-3} M, 193 K, ppm), δ -115.9 (*o*-F, br m), -164.3 (*m*-F, br m), -164.6 (*p*-F, br m), -166.7 (*m*-F, br m), -166.9 (*p*-F, br m). ^{195}Pt{^{1}H} NMR (Acetone-d_6, 295 K, ppm), δ –3052 (m). Λ_M (Acetone): 118 $\Omega^{-1}cm^{-2}mol^{-1}$.

Synthesis of [{Pt(bzq)(C_6F_5)$_2$}$_2$Pb] (3). To a solution of $PbClO_4 \cdot 3H_2O$ (0.032 g, 0.079 mmol) in acetone (10 mL) $(NBu_4)[Pt(bzq)(C_6F_5)_2]$ (0.150 g, 0.158 mmol) was added. After 40 minute of stirring in absence of light the solution was **3** crystallized. The yellow-orange solid was filtered off, washed with cold acetone (3 × 1 mL) and dried-vacuum, 0.085g, 67% yield. Anal. Found (calcd for $C_{50}H_{16}F_{20}N_2Pt_2Pb$): C, 36.81 (37.02); H, 1.23 (0.99); N, 1.74 (1.73). MALDI-TOF (+): *m/z* (%) 913 $[Pt(bzq)(C_6F_5)_2Pb]^+$ (33), 1454 $[Pt_2(bzq)_2(C_6F_5)_3Pb]^+$ (13). IR (cm^{-1}): 1635(w), 1617(w), 1605(w), 1504(m), 1059(m), 949 (s), 836 (m), 822 (s), 803 (m), 780 (m, C_6F_5, X-sensitive vibr.),[116] 759 (m, C_6F_5, X-sensitive vibr.),[116] 652 (s). ^{1}H NMR (Acetone-d_6, 295 K, ppm), δ 8.61 (H4, d, $^3J_{H(4),H(3)}$ = 7.8 Hz), 8.56 (H2, d, $^3J_{H(2),H(3)}$ = 5.1 Hz, $^3J_{H(2),Pt}$ = 25 Hz), 7.90 (H5, d, $^3J_{H(5),H(6)}$ = 8.7 Hz), 7.83 (H6, d, $^3J_{H(6),H(5)}$ = 9.0 Hz), 7.67 (H7, d, $^3J_{H(7),H(8)}$ = 8.1 Hz), 7.6 (H3, dd, $^3J_{H(3),H(4)}$ = 7.82 Hz, $^3J_{H(3),H(2)}$ = 5.1 Hz), 7.30 (H8, dd, $^3J_{H(8),H(7)}$ = 7.5 Hz, $^3J_{H(8),H(9)}$ = 6.9 Hz), 7.12 (H9, d, $^3J_{H(9),H(8)}$ = 6.9 Hz, $^3J_{H(9),Pt}$ = 38 Hz). ^{19}F NMR (Acetone-d_6, 295 K, ppm), δ –115.1 (*o*-F, br d), –118.7 (*o*-F, br d), –163.8 (F,

s), −167.4 (F,s), −165.8 (F, s), −166.3 (F,s). Its low solubility prevented characterization by $^{195}Pt\{^{1}H\}$ NMR spectroscopy. Λ_M (Acetone): 35 $\Omega^{-1}cm^{-2}mol^{-1}$.

X-ray structure determinations. Crystal data and other details of the structure analyses are presented in Table S5. Suitable crystals for X-ray diffraction studies were obtained by slow diffusion of *n*-hexane into concentrated solutions of the complexes in 3 mL of Me_2CO (**1**·n0.5Me_2CO·n0.25*n*-C_6H_{14}, and **3**), CH_2Cl_2 [**2**·0.75CH_2Cl_2 (**2a**), **2**·CH_2Cl_2 (**2b**)] or THF [**2·THF** (**2c**)]. Crystals were mounted at the end of a quartz fibre. The radiation used in all cases was graphite monochromated MoK_α (λ = 0.71073 Å). For **1**·n0.5Me_2CO·n0.25*n*-C_6H_{14}, **2**·0.75CH_2Cl_2, **2**·CH_2Cl_2 and **3**, X-ray intensity data were collected on an Oxford Diffraction Xcalibur diffractometer and the diffraction frames were integrated and corrected from absorption by using the CrysAlis RED program.[117] For **2·THF**, X-ray intensity data were collected with a NONIUS-κCCD area-detector diffractometer and images processed using the DENZO and SCALEPACK suite of programs,[118] and the absorption correction was performed using SORTAV.[119]

The structures were solved by Patterson and Fourier methods and refined by full-matrix least squares on F^2 with SHELXL-97.[120] All non-hydrogen atoms were assigned anisotropic displacement parameters and refined without positional constraints, except as noted below. All hydrogen atoms were constrained to idealized geometries and assigned isotropic displacement parameters equal to 1.2 times the U_{iso} values of their attached parent atoms (1.5 times for the methyl hydrogen atoms).

In the structure of **1**·n1.5Me_2CO·n0.25*n*-C_6H_{14}, one of the bzq ligands is disordered over two sets of positions which were refined with partial occupancy 0.7/0.3. Weak restraints were applied over the geometry of these moieties and the equivalent atoms of both were refined with common anisotropic displacement parameters. Moreover, a very diffuse molecule of *n*-hexane was found during the refinement and the occupancy of its atoms was fixed to 0.3. Geometric parameters for this molecule were restrained to acceptable values. For **2**·0.75CH_2Cl_2 (**2a**, monoclinic, $P2_1/n$) very diffuse solvent was found in the final stages of the refinement and modelled as a two dichloromethane molecules with partial occupancy of 0.50 and 0.75. Geometric parameters for these molecules were restrained to acceptable values. **2**·CH_2Cl_2 (**2b**, monoclinic $P2_1/c$), includes a full CH_2Cl_2 molecules in the asymmetric part of the unit cell. In this, a terminal CH_2-CH_3 fragment of the tetrabutylammonium cation was found

to be disordered and the disorder modelled as two sites with partial occupancy 0.6/0.4. Constraints were applied on the geometry and the anisotropic displacement parameters of these C atoms. **2·THF** (**2c**, orthorrombic *Pbca*), includes a THF molecule coordinated to the Tl center. In the structure of **3**, some very diffuse and minor electron residual density was present without a clear chemical meaning. After several attempts to model this density as oxygen water atoms, with very low occupancy and not very convincing results, the SQUEEZE procedure as implemented in PLATON[121] was used giving rise to satisfactory results. Full-matrix least-squares refinement of these models against F^2 converged to final residual indices given in Table S5.

Supporting Information. Crystal and structural data for compounds **1**·n0.5Me_2CO·n0.25*n*-C_6H_{14}, **2**·0.75CH_2Cl_2 (**2a**), **2**·CH_2Cl_2 (**2b**), **2**·THF (**2c**), and **3** both in tabular and CIF format; additional Figures and Tables with information of ^{19}F NMR spectroscopy and photophysical properties of the complexes described in this paper. This material is available free of charge via the Internet at http://pubs.acs.org.

Acknowledgment. This work was supported by the Spanish MICINN (DGPTC/FEDER) (Project CTQ2008-06669-C02-01-02/BQU) and MINECO/FEDER (Projects Nos. CTQ2012-35251 and CTQ2013-45518-P) and the Gobierno de Aragón (Grupo Consolidado E21: Quı́mica Inorgánica y de los Compuestos Organometálicos).

References

(1) Pyykkö, P. *Chem. Rev.* **1997**, *97*, 597-636.

(2) Pyykkö, P. *Angew. Chem. Int. Ed.* **2004**, *43*, 4412-4456.

(3) Gade, L. H. *Angew. Chem. Int. Ed.* **2001**, *40*, 3573-3575.

(4) Carvajal, M. A.; Álvarez, S.; Novoa, J. J. *Chem, Eur. J.* **2004**, *10*, 2117-2132.

(5) Díez, A.; Lalinde, E.; Moreno, M. T. *Coord. Chem. Rev.* **2011**, *255*, 2426-2447.

(6) Fernández, E. J.; Laguna, A.; López de Luzuriaga, J. M. *Dalton Trans.* **2007**, 1969-1981.

(7) Fernández, E. J.; López de Luzuriaga, J. M.; Monge, M.; Rodríguez, M. A.; Crespo, O.; Gimeno, M. C.; Laguna, A.; Jones, P. G. *Chem, Eur. J.* **2000**, *6*, 636-644.

(8) Yam, V. W. W.; Cheng, E. C. C. *Chem. Soc. Rev.* **2008**, *37*, 1806-1813.

(9) Schmidbaur, H.; Schier, A. *Chem. Soc. Rev.* **2008**, *37*, 1931-1951.

(10) Sculfort, S.; Braunstein, P. *Chem. Soc. Rev.* **2011**, *40*, 2741-2760.

(11) Fernández, E. J.; Laguna, A.; López de Luzuriaga, J. M. *Coord. Chem. Rev.* **2005**, *249*, 1423-1433.

(12) Moret, M.-E.; Chen, P. *J. Am. Chem. Soc.* **2009**, *131*, 5675-5690.

(13) Forniés, J.; Ibáñez, S.; Martín, A.; Sanz, M.; Berenguer, J. R.; Lalinde, E.; Torroba, J. *Organometallics* **2006**, *25*, 4331-4340.

(14) Forniés, J.; Ibáñez, S.; Martín, A.; Gil, B.; Lalinde, E.; Moreno, M. T. *Organometallics* **2004**, *23*, 3963-3975.

(15) Yamaguchi, T.; Yamazaki, F.; Ito, T. *J. Am. Chem. Soc.* **1999**, *121*, 7405-7406.

(16) Falvello, L. R.; Forniés, J.; Garde, R.; García, A.; Lalinde, E.; Moreno, M. T.; Steiner, A.; Tomás, M.; Usón, I. *Inorg. Chem.* **2006**, *45*, 2543-2552.

(17) Berenguer, J. R.; Díez, A.; Fernández, J.; Forniés, J.; García, A.; Gil, B.; Lalinde, E.; Moreno, M. T. *Inorg. Chem.* **2008**, *47*, 7703-7716.

(18) Falvello, L. R.; Forniés, J.; Martín, A.; Sicilia, V.; Villarroya, P. *Organometallics* **2002**, *21*, 4604-4610.

(19) Alonso, E.; Forniés, J.; Fortuño, C.; Martín, A.; Orpen, A. G. *Organometallics* **2003**, *22*, 5011-5019.

(20) Rochon, F. D.; Melanson, R. *Acta Cryst. Sect. C: Cryst. Struct. Commun.* **1988**, *44*, 474-477.

(21) Forniés, J.; Fuertes, S.; Martín, A.; Sicilia, V.; Gil, B.; Lalinde, E. *Dalton Trans.* **2009**, 2224-2234.

(22) Casas, J. M.; Forniés, J.; Fuertes, S.; Martín, A.; Sicilia, V. *Organometallics* **2007**, *26*, 1674-1685.

(23) Falvello, L. R.; Forniés, J.; Fortuño, C.; Durán, F.; Martín, A. *Organometallics* **2002**, *21*, 2226-2234.

(24) Ara, I.; Falvello, L. R.; Forniés, J.; Gómez, J.; Lalinde, E.; Merino, R. I.; Usón, I. *J. Organomet. Chem.* **2002**, *663*, 284-288.

(25) Falvello, L. R.; Forniés, J.; Lalinde, E.; Menjón, B.; García Monforte, M. A.; Moreno, M. T.; Tomás, M. *Chem. Commun.* **2007**, 3838-3840.

(26) Yamaguchi, T.; Yamazaki, F.; Ito, T. *J. Am. Chem. Soc.* **2001**, *123*, 743-744.

(27) Forniés, J.; Ibáñez, S.; Lalinde, E.; Martín, A.; Moreno, M. T.; Tsipis, A. C. *Dalton Trans.* **2012**, *41*, 3439-3451.

(28) Fuertes, S.; Woodall, C. H.; Raithby, P. R.; Sicilia, V. *Organometallics* **2012**, *31*, 4228-4240.

(29) Belío, Ú.; Fuertes, S.; Martín, A. *Inorg. Chem.* **2013**, *52*, 5627-5629.

(30) Martín, A.; Belío, U.; Fuertes, S.; Sicilia, V. *Eur. J. Inorg. Chem.* **2013**, 2231-2247.

(31) Chou, P. T.; Chi, Y. *Chem. Eur. J.* **2007**, *13*, 380-395.

(32) Cooke, M. W.; Hanan, G. S. *Chem. Soc. Rev.* **2007**, *36*, 1466-1476.

(33) Evans, R. C.; Douglas, P.; Wiscom, C. J. *Coord. Chem. Rev.* **2006**, *250*, 2093-2126.

(34) Holder, E.; Langeveld, B. M. W.; Schubert, U. S. *Adv. Mater.* **2005**, *17*, 1109-1121.

(35) McClenaghan, M. D.; Leydet, N. D.; Maubert, Y.; Indelli, M. T.; Campagna, S. *Coord. Chem. Rev.* **2005**, *249*, 1336-1350.

(36) Sun, S. S.; Lees, A. J. *Coord. Chem. Rev.* **2002**, *230*, 171-192.

(37) Wong, W. Y. *Comments Inorg. Chem.* **2005**, *26*, 39-74.

(38) Huynh, M. H. V.; Dattelbaum, D. M.; Meyer, T. J. *Coord. Chem. Rev.* **2005**, *249*, 457-483.

(39) Vogler, A.; Kunkely, H. *Top. Curr. Chem.* **2001**, *213*, 143-182.

(40) Thanasekaran, P.; Liao, R. T.; Liu, Y. H.; Rajendran, T.; Rajagopal, S.; Lu, K. L. *Coord. Chem. Rev.* **2005**, *249*, 1085-1110.

(41) *Coord. Chem. Rev.* **2000**, *208 (special issue)*, 1-371.

(42) Ma, B.; Djurovich, P. I.; Thompson, M. E. *Coord. Chem. Rev.* **2005**, *249*, 1501-1510 and references therein.

(43) Pérez, S.; López, C.; Caubet, A.; Bosque, R.; Solans, X.; Bardía, M. F.; Roig, A.; Molins, E. *Organometallics* **2004**, *23*, 224-236 and references therein.

(44) Kobayashi, A.; Kato, M. *Eur. J. Inorg. Chem.* **2014**, *2014*, 4469-4483.

(45) Wenger, O. S. *Chem. Rev.* **2013**, *113*, 3686-3733.

(46) Zhang, X.; Li, B.; Chen, Z.-H.; Chen, Z.-N. *J. Mater. Chem.* **2012**, *22*, 11427-11441.

(47) Zhao, Q.; Li, F.; Huang, C. *Chem. Soc. Rev.* **2010**, *39*, 3007-3030.

(48) Berenguer, J. R.; Lalinde, E.; Martín, A.; Moreno, M. T.; Ruiz, S.; Sánchez, S.; Shahsavari, H. R. *Inorg. Chem.* **2014**, *53*, 8770-8785.

(49) Forniés, J.; Martín, A. In *Metal Clusters in Chemistry*; Braunstein, P., Oro, L. A., Raithby, P. R., Eds.; Wiley-VCH: Weinheim, 1999; Vol. 1, pp 417-443.

(50) Forniés, J.; Fortuño, C.; Ibáñez, S.; Martín, A. *Inorg. Chem.* **2008**, *47*, 5978-5987.

(51) Forniés, J.; Gómez, J.; Lalinde, E.; Moreno, M. T. *Inorg. Chem.* **2001**, *40*, 5415-5419.

(52) Casas, J. M.; Forniés, J.; Martín, A.; Menjón, B.; Tomás, M. *Polyhedron* **1996**, *15*, 3599-3604.

(53) Chen, W.; Liu, F.; Nishioka, T.; Matsumoto, K. *Eur. J. Inorg. Chem.* **2003**, 4234-4243.

(54) Díez, A.; Forniés, J.; Gómez, J.; Lalinde, E.; Martín, A.; Moreno, M. T.; Sánchez, S. *Dalton Trans.* **2007**, 3653-3660.

(55) Kampf, G.; Miguel, P. J. S.; Willermann, M.; Schneider, A.; Lippert, B. *Chem. Eur. J.* **2008**, *14*, 6882-6891.

(56) Song, H. B.; Zhang, Z.-Z.; Hui, Z.; Che, C.-M.; Mak, T. C. W. *Inorg. Chem.* **2002**, *41*, 3146-3154.

(57) Janzen, D. E.; Mehne, L. F.; VanDerveer, D. G.; Grant, G. J. *Inorg. Chem.* **2005**, *44*, 8182-8184.

(58) Baudron, S. A.; Hosseini, M. W. *Chem. Commun.* **2008**, 4558-4560.

(59) Yin, G.-Q.; Wei, Q.-H.; Zhang, L.-Y.; Chen, Z.-N. *Organometallics* **2006**, *25*, 580-587.

(60) Xia, B.-H.; Zhang, H.-X.; Che, C.-M.; Leung, K.-H.; Phillips, D.-L.; Zhu, N.; Zhou, Z.-Y. *J. Am. Chem. Soc.* **2003**, *125*, 10362-10374.

(61) Moret, M.-E.; Chen, P. *Organometallics* **2008**, *27*, 4903-4916.

(62) Ara, I.; Falvello, L. R.; Forniés, J.; Sicilia, V.; Villarroya, P. *Organometallics* **2000**, *19*, 3091-3099.

(63) Ara, I.; Forniés, J.; Sicilia, V.; Villarroya, P. *Dalton Trans.* **2003**, 4238-4242.

(64) Usón, R.; Forniés, J.; Tomás, M.; Garde, R.; Alonso, P. J. *J. Am. Chem. Soc.* **1995**, *117*, 1837-1838.

(65) Baya, M.; Belío, Ú.; Forniés, J.; Martín, A.; Perálvarez, M.; Sicilia, V. *Inorg. Chim. Acta* **2015**, *424*, 136-149.

(66) Usón, R.; Forniés, J.; Tomás, M.; Garde, R.; Merino, R. *Inorg. Chem.* **1997**, *36*, 1383-1387.

(67) Balch, A. L.; Rowley, S. P. *J. Am. Chem. Soc.* **1990**, *112*, 6139-6140.

(68) Oberbeckmann-Winter, N.; Braunstein, P.; Welter, R. *Organometallics* **2004**, *23*, 6311-6318.

(69) Nagle, J. K.; Balch, A. L.; Olmstead, M. M. *J. Am. Chem. Soc.* **1988**, *110*, 319-321.

(70) Charmant, J. P. H.; Forniés, J.; Gómez, J.; Lalinde, E.; Merino, R. I.; Moreno, M. T.; Orpen, A. G. *Organometallics* **2003**, *22*, 652-656.

(71) Liu, F.; Chen, W.; Wang, D. *Chin. J. Struct. Chem.* **2006**, *25*, 677-680.

(72) Berenguer, J. R.; Fernández, J.; Lalinde, E.; Sánchez, S. *Chem. Commun* **2012**, *48*, 6384-6386.

(73) Renn, O.; Lippert, B.; Mutikainen, I. *Inorg. Chim. Acta* **1993**, *208*, 219-223.

(74) Chen, W.; Liu, F.; Xu, D. X.; Matsumoto, K.; Kishi, S.; Kato, M. *Inorg. Chem.* **2006**, *45*, 5552-5560.

(75) Stork, J. R.; Olmstead, M. M.; Fettinger, J. C.; Balch, A. L. *Inorg. Chem.* **2006**, *45*, 849-857.

(76) Forniés, J.; García, A.; Lalinde, E.; Moreno, M. T. *Inorg. Chem.* **2008**, *47*, 3651-3660.

(77) Stork, J. R.; Olmstead, M. M.; Balch, A. L. *J. Am. Chem. Soc.* **2005**, *127*, 6512-6513.

(78) Díez, A.; Fernández, J.; Lalinde, E.; Moreno, M. T.; Sánchez, S. *Inorg. Chem.* **2010**, *49*, 11606-11618.

(79) Belío, Ú.; Fuertes, S.; Martín, A. *Dalton Trans.* **2014**, *43*, 10828-10843.

(80) Berenguer, J. R.; Forniés, J.; Gil, B.; Lalinde, E. *Chem. Eur. J.* **2006**, *12*, 785-795.

(81) Wu, G.; Wang, D. *J. Cluster Sci.* **2007**, *18*, 406-413.

(82) Balch, A. L.; Fung, E. Y.; Nagle, J. K.; Olmstead, M. M.; Rowley, S. P. *Inorg. Chem.* **1993**, *32*, 3295-3299.

(83) Usón, R.; Forniés, J.; Falvello, L. R.; Usón, M. A.; Usón, I. *Inorg. Chem.* **1992**, *31*, 3697-3698.

(84) Albano, V. G.; Castellari, C.; Monari, M.; DeFelice, V.; Ferrara, M. L.; Ruffo, F. *Organometallics* **1995**, *14*, 4213-4221.

(85) Casas, J. M.; Forniés, J.; Martín, A.; Orera, V. M.; Orpen, A. G.; Rueda, A. *Inorg. Chem.* **1995**, *34*, 6514-6519.

(86) Berenguer, J. R.; Fernández, J.; Gil, B.; Lalinde, E.; Sánchez, S. *Chem. Eur. J.* **2014**, *20*, 2574-2584.

(87) Berenguer, J. R.; Lalinde, E.; Martín, A.; Moreno, M. T.; Ruiz, S.; Sánchez, S.; Shahsavari, H. R. *Chem. Commun.* **2013**, *49*, 5067-5069.

(88) Shimoni-Livny, L.; Glusker, J. P.; Bock, C. W. *Inorg. Chem.* **1998**, *37*, 1853-1867.

(89) Davidovich, R. L.; Stavila, V.; Marinin, D. V.; Voit, E. I.; Whitmire, K. H. *Coord. Chem. Rev.* **2009**, *253*, 1316-1352.

(90) Davidovich, R. L.; Stavila, V.; Whitmire, K. H. *Coord. Chem. Rev.* **2010**, *254*, 2193-2226.

(91) Gourlaouen, C.; Gérard, H.; Piquemal, J.-P.; Parisel, O. *Chem. Eur. J.* **2008**, *14*, 2730-2743.

(92) Greer, B. J.; Michaelis, V. K.; Katz, M. J.; Leznoff, D. B.; Schreckenbach, G.; Kroeker, S. *Chem. Eur. J.* **2011**, *17*, 3609-3618.

(93) Jamali, S.; Ghazfar, R.; Lalinde, E.; Jamshidi, Z.; Samouei, H.; Shahsavari, H. R.; Moreno, M. T.; Escudero-Adan, E.; Benet-Buchholz, J.; Milic, D. *Dalton Trans.* **2014**, *43*, 1105-1116.

(94) Ara, I.; Berenguer, J. R.; Forniés, J.; Gómez, J.; Lalinde, E.; Martín, A.; Merino, R. *Inorg. Chem.* **1997**, *36*, 6461-6464.

(95) Bondi, A. *J. Phys. Chem.* **1964**, *68*, 441.

(96) Fernández, E. J.; Laguna, A.; López de Luzuriaga, J. M.; Mendizábal, F.; Monge, M.; Olmos, M. E.; Pérez, J. *Chem, Eur. J.* **2003**, *9*, 456-465.

(97) Braga, D.; Grepioni, F. *Chem. Soc. Rev.* **2000**, *29*, 229-238.

(98) Fernández, E. J.; López de Luzuriaga, J. M.; Monge, M.; Montiel, M.; Olmos, M. E.; Pérez, J.; Laguna, A.; Mendizábal, F.; A., M. A.; Fackler, J. P. *Inorg. Chem.* **2004**, *43*, 3573-3581.

(99) de Silva, N.; Fry, C. G.; Dahl, L. F. *Dalton Trans.* **2006**, 1051-1059.

(100) Childress, M. V.; Millar, D.; Alam, T. M.; Kreisel, K. A.; Yap, G. P. A.; Zakharov, L. N.; Golen, J. A.; Rheingold, A. L.; Doerrer, L. H. *Inorg. Chem.* **2006**, *45*, 3864-3877.

(101) Dick, A. R.; Kampf, J. W.; Sanford, M. S. *Organometallics* **2005**, *24*, 482-485.

(102) De Priest, J.; Zheng, G. Y.; Woods, C.; Rillema, D. P.; Mikirova, N. A.; Zandler, M. E. *Inorg. Chim. Acta* **1997**, *264*, 287-296.

(103) Godbert, N.; Pugliese, T.; Aiello, I.; Bellusci, A.; Crispini, A.; Ghedini, M. *Eur. J. Inorg. Chem.* **2007**, 5105-5111.

(104) Díez, A.; Forniés, J.; García, A.; Lalinde, E.; Moreno, M. T. *Inorg. Chem.* **2005**, *44*, 2443-2453.

(105) Jolliet, P.; Gianini, M.; von Zelewsky, A.; Bernardinelli, G.; Stoeckli-Evans, H. *Inorg. Chem.* **1996**, *35*, 4883-4888.

(106) Janzen, D. E.; VanDerveer, D. G.; Mehne, L. F.; da Siva Filho, D. A.; Bredas, J. L.; Grant, G. J. *Dalton Trans.* **2008**, 1872-1882.

(107) Shannon, R. D. *Acta Crystallogr.* **1976**, *A32*, 751-767.

(108) Dolg, M.; Pyykkö, P.; Runeberg, N. *Inorg. Chem.* **1996**, *35*, 7450-7451.

(109) Houlding, V. H.; Miskoswski, V. M. *Coord. Chem. Rev.* **1991**, *111*, 145-152.

(110) Zheng, G. Y.; Rillema, D. P. *Inorg. Chem.* **1998**, *37*, 1392-1397.

(111) Forniés, J.; Fuertes, S.; Martín, A.; Sicilia, V.; Lalinde, E.; Moreno, M. T. *Chem. Eur. J.* **2006**, *12*, 8253.

(112) Strasser, C. E.; Catalano, V. J. *J. Am. Chem. Soc.* **2010**, *132*, 10009-10011.

(113) Ley, A. N.; Dunaway, L. E.; Brewster, T. P.; Dembo, M. D.; Harris, T. D.; Baril-Robert, F.; Li, X.; Patterson, H. H.; Pike, R. D. *Chem. Commun.* **2010**, *46*, 4565-4567.

(114) Supriya, S.; Das, S. K. *J. Am. Chem. Soc.* **2007**, *129*, 3464-3465.

(115) Lefebvre, J.; Korcok, J. L.; Katz, M. J.; Leznoff, D. B. *Sensors* **2012**, *12*, 3669-3692.

(116) Maslowsky, E. J. *Vibrational Spectra of Organometallic Compounds*; Wiley: New York, 1977.

(117) CrysAlis RED, CCD camera data reduction program, Oxford Diffraction: Oxford, UK, 2004.

(118) Otwinowski, Z.; Minor, W. *Methods Enzymol. A: Macromol. Crystallogr.* **1997**, *276*, 307-326.

(119) Blessing, R. H. *Acta Cryst.* **1995**, *A51*, 33-38.

(120) Sheldrick, G. M. *Acta Cryst.* **2008**, *A64*, 112-122.

(121) Spek, A. L. *PLATON, A Multipurpose Crystallographic Tool*; Utrecht University: Utrecht, the Netherlands, 2010.

Table 1. Selected bond lengths (Å) and angles (°) around the metal (Tl or Pb) for $[\{Pt(bzq)(C_6F_5)_2\}Tl(Me_2CO)]_n \cdot n0.5Me_2CO \cdot n0.25n\text{-}C_6H_{14}$ (**1**·n0.5Me_2CO·n0.25*n*-C_6H_{14}), $(NBu_4)[\{Pt(bzq)(C_6F_5)_2\}_2Tl]$ [**2**·0.75CH_2Cl_2 (**2a**), **2**·CH_2Cl_2 (**2b**) and **2**·THF (**2c**)] and $[\{Pt(bzq)(C_6F_5)_2\}_2Pb]$ (**3**)

1·n0.5Me_2CO·n0.25*n*-C_6H_{14}			
Pt(1)–Tl(1)	2.9609(3)	Pt(1)–Tl(2)	2.9945(3)
Pt(2)–Tl(1')	2.9301(3)	Pt(2)–Tl(2)	3.0666(3)
Tl(1)···F(1)	3.027(4)	Tl(1)···F(6)	3.057(4)
Tl(2)···F(5)	3.048(4)	Tl(2)···F(10)	3.091(3)
Tl(2)···F(15)	3.056(4)	Tl(2)···F(20)	3.083(4)
Tl(1)–O(1)	2.805(6)	Tl(2)–O(2)	2.720(5)
Pt(1)–Tl(2)–Pt(2)	150.179(11)	Pt(2')–Tl(1)–Pt(1)	154.931(10)
Tl(1)–Pt(1)–Tl(2)	159.81(1)	Tl(1")–Pt(2)–Tl(2)	149.091(11)

	2·0.75CH_2Cl_2 (**2a**)	**2**·CH_2Cl_2 (**2b**)	**2**·THF (**2c**)
Pt(1)–Tl	2.8815(4)	2.9254(3)	2.9352(6)
Pt(2)–Tl	2.9432(4)	2.8747(3)	2.9705(6)
Tl(1)···F(1)	2.976(6)	2.850(4)	3.141(3)
Tl(1)···F(10)	3.205(5)	3.201(4)	3.106(3)
Tl(1)···F(15)	2.901(6)	2.951(4)	3.154(3)
Tl(1)···F(16)	3.150(4)	3.016(3)	3.255(3)
Tl–O	-	-	2.630(4)
Pt(1)–Tl–Pt(2)	150.65(2)	146.91(1)	155.91(1)

3			
Pt–Pb	2.7757(3)	Pt'–Pb–Pt	150.26(2)
Pb···F(1)	2.972(4)	Pb···F(6)	2.792(5)

Table 2. Absorption data for compounds **1**-**3** at 298 K

Compound	**λ_{abs} / nm (10^3 ε $M^{-1}cm^{-1}$) (solution ~ 5 x 10^{-5} M)**
$[NBu_4][Pt(bzq)(C_6F_5)_2]$ (**A**)	243 (46.9), 262 (40.3), 317 (11.0), 352 (8.4), 399 (5.6), 448 (2.5) **THF**[ref27] 243 (66.4), 260 (58.4), 315 (27.5), 345 (20.1), 380 (12.1), 425 (6.9) **CH_2Cl_2**[ref13] 265, 310, 357, 392, 434, 472 **solid**[ref27]
$[\{Pt(bzq)(C_6F_5)_2\}Tl(Me_2CO)]_n$ (**1**)	240 (28.8), 283 (12.6), 307 (9.5), 373 (2.9), 415 (1.8) **THF** 235 (47.5), 302 (19.6), 367 (6.6), 410 (3.6) **CH_2Cl_2** 256, 306, 412, 480, 505, 530sh, 550sh, tail to 600 **solid**
$[NBu_4][\{Pt(bzq)(C_6F_5)_2\}_2Tl]$ (**2**)	260 (30.0), 311 (11.1), 353 (7.5), 406 (4.8) **THF** 235 (50.1), 264 (40.1), 308 (14.0), 343 (9.0), 391 (5.0), 430 (2.5) **CH_2Cl_2** 268, 309, 360, 430, 462sh, tail to 540 **solid**
$[\{Pt(bzq)(C_6F_5)_2\}_2Pb]$ (**3**)	238 (30.6), 283 (11.1), 310 (8.5), 338 (6.6), 367 (3.4), 416 (1.6) **THF** 237 (58.4), 284 (26.4), 315 (19,6), 354 (12.0), 386 (8.4),440 (5.7), 511 (2.7), tail to 555 **CH_2Cl_2** 245, 305, 365, 437, 455, 480sh, 515sh, tail to 540, **solid**

Table 3. Photophysical data for complexes **1**-**3** in solid state

Compound	**(*T*/K)**	**λ_{em}/nm (λ_{exc}/nm) [ϕ/%]**	**τ/μs**	**K_r[a]**	**K_{nr}[b]**
1	298	610 (365-480) [28.4]	0.2 (66%), 0.6 (34%)	8.5×10^5	2.1×10^6
1	77	685 (400-480)	10.0		
1-grinding	298	665 (420-450) [2.4]	0.1 (20%), 0.7 (80%)	4.1×10^4	1.7×10^6
1-grinding	77	685 (420-450)	8.6 (11%), 2.9 (89%)		
1-THF	298	560 (365-420) [19.3]	0.1 (37%), 0.9 (63%)	3.2×10^5	1.3×10^6
1-THF	77	618 (420)	10.8 (7%), 2.9 (93%)		
1-Et_2O	298	577 (420) [44.4]	1.1 (41%), 0.4 (59%)	6.5×10^5	8.1×10^5
1-Et_2O	77	617 (420)	10.3 (46%), 3.6 (54%)		
2	298	615 (400-450) [31.7]	1.5	2.1×10^5	4.5×10^5
2	77	512, 554, 640_{max} (440)	41.1 (512)		
		640 (480)	11.0		
2-Me_2CO	298	595 (420) [30.3]	0.3	1.0×10^6	2.3×10^6
2-Me_2CO	77	615 (440)	9.6		
2-THF	298	590 (420) [0.4]	0.2	2.0×10^4	5.0×10^6
2-THF	77	595-605 (440)	21.0 (38%), 132.6 (62%) (605)		
2-Et_2O	298	588 (420) [20.1]	2.1	9.6×10^4	3.8×10^5
2-Et_2O	77	590[c] (440)	9.5		
3	298	547 (365-450) [20]	0.02 (44%), 0.5 (56.1%)	6.9×10^5	2.8×10^6
3	77	547 (365-450)	61.7		

[a] $K_r = \phi/\tau_{average;}$ [b] $K_{nr} = (1-\phi)/\tau_{average;}$ [c] The weak band at 512 nm is still observed

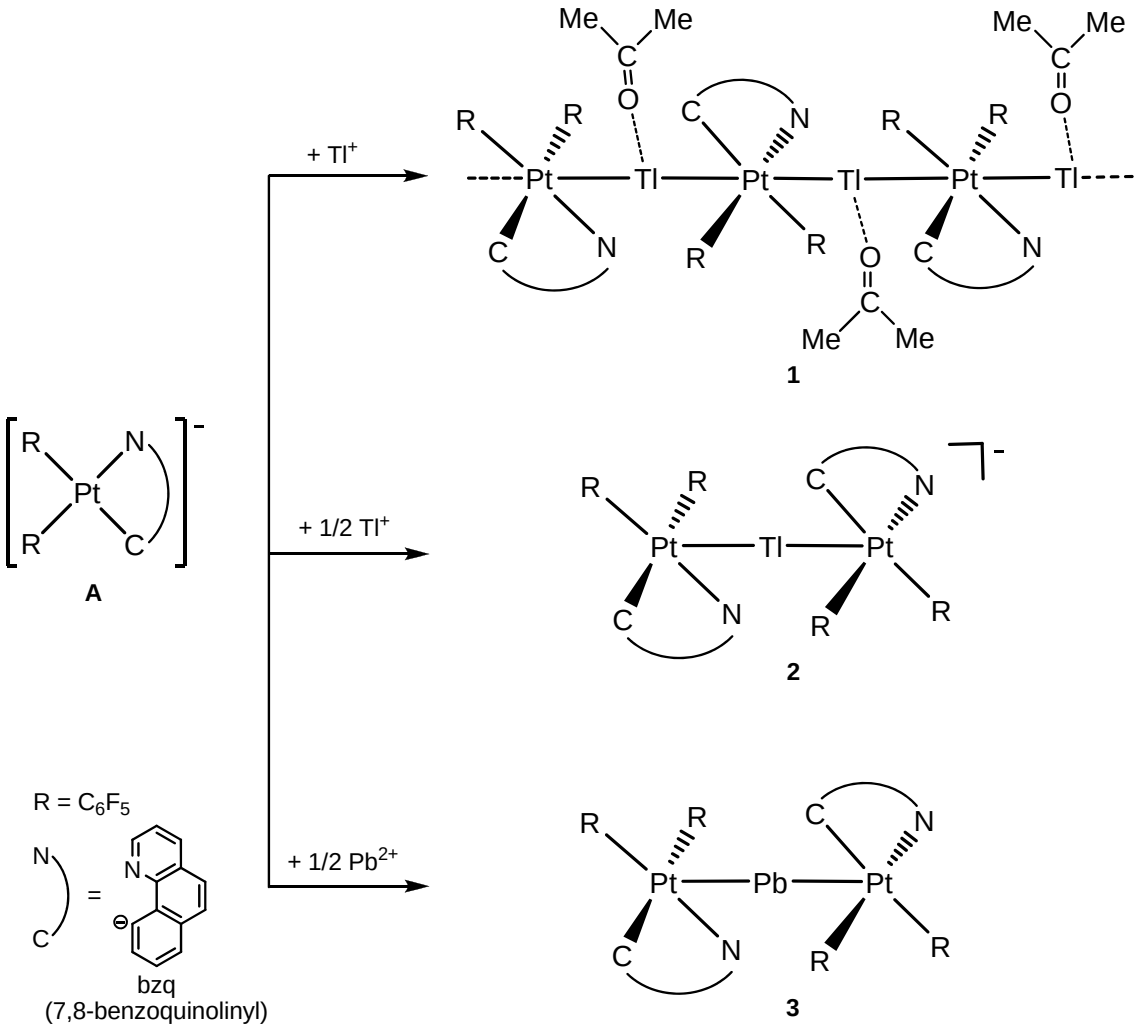

Scheme 1

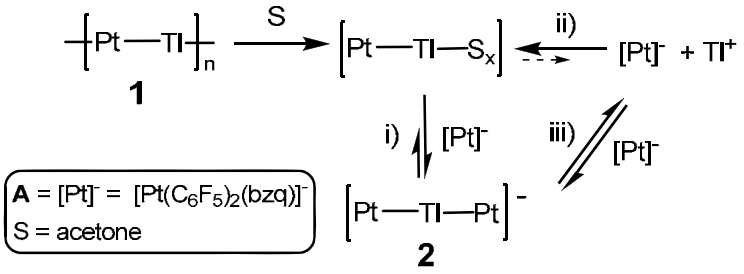
Pt—Tl
n
1
S
Pt—Tl—Sx
ii)
[Pt]- + Tl+
i)
[Pt]-
iii)
[Pt]-
A = [Pt]- = [Pt(C6F5)2(bzq)]-
S = acetone
Pt—Tl—Pt
-
2

Scheme 2

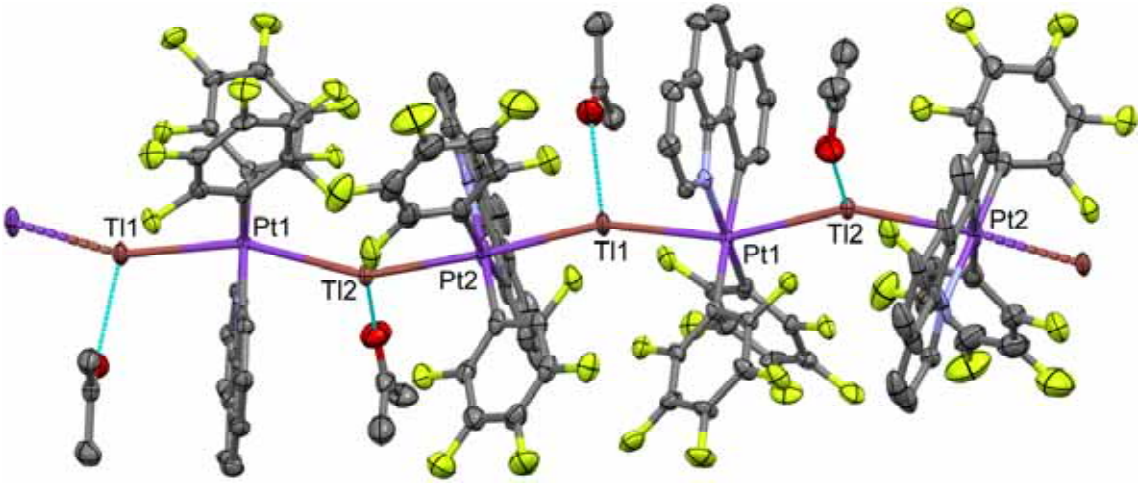

a

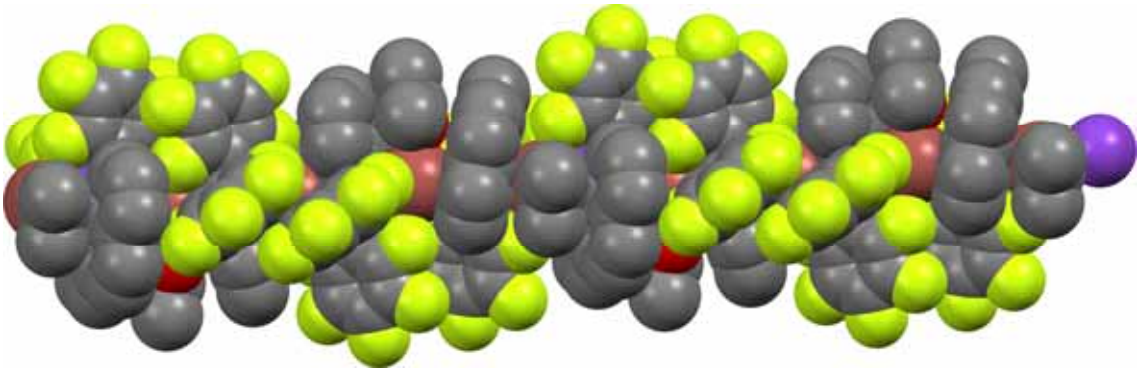

b

Figure 1. a) View of the molecular structure of $[\{Pt(bzq)(C_6F_5)_2\}Tl(Me_2CO)]_n \cdot n0.5Me_2CO \cdot n0.25n\text{-}C_6H_{14}$ (**1**$\cdot n0.5Me_2CO \cdot n0.25n\text{-}C_6H_{14}$). Ellipsoids are drawn at their 50% probability level. b) View of the helical arrangement of the infinite chain

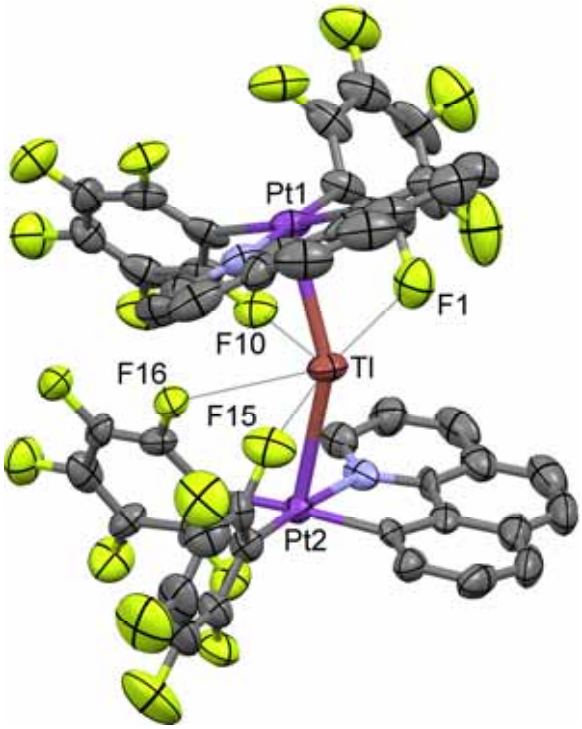

a

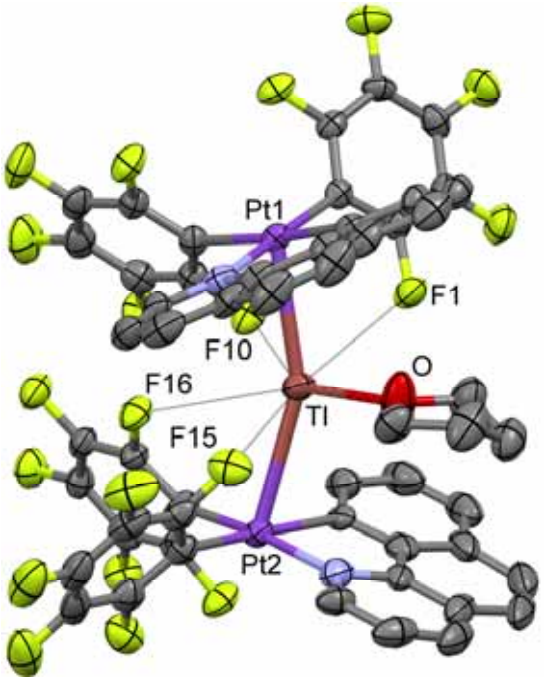

b

Figure 2. View of the molecular structures of the complex anion of $(NBu_4)[\{Pt(bzq)(C_6F_5)_2\}_2Tl]$ as found in the forms **2a** (a) and **2c** (b). Ellipsoids are drawn at their 50% probability level

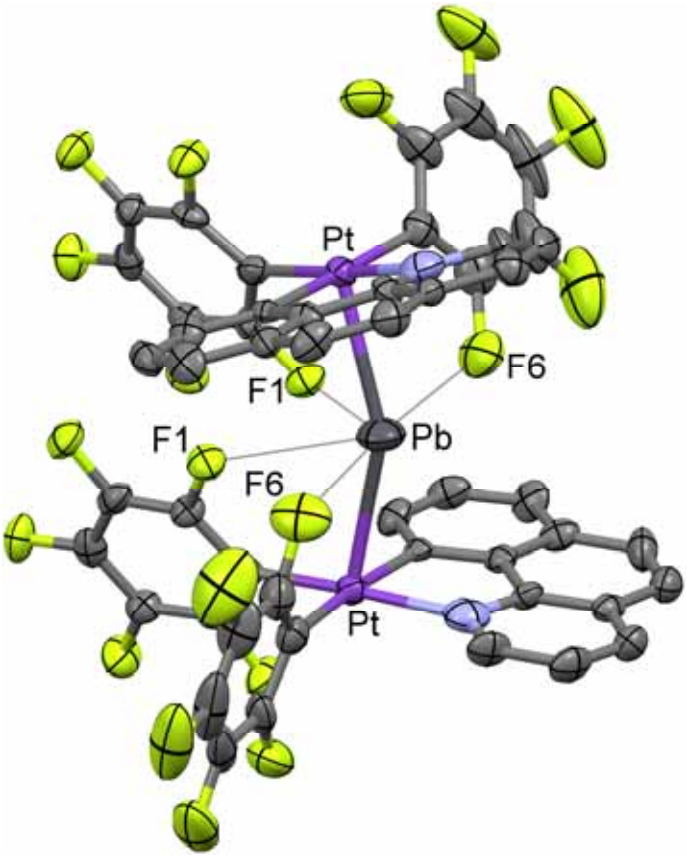

a

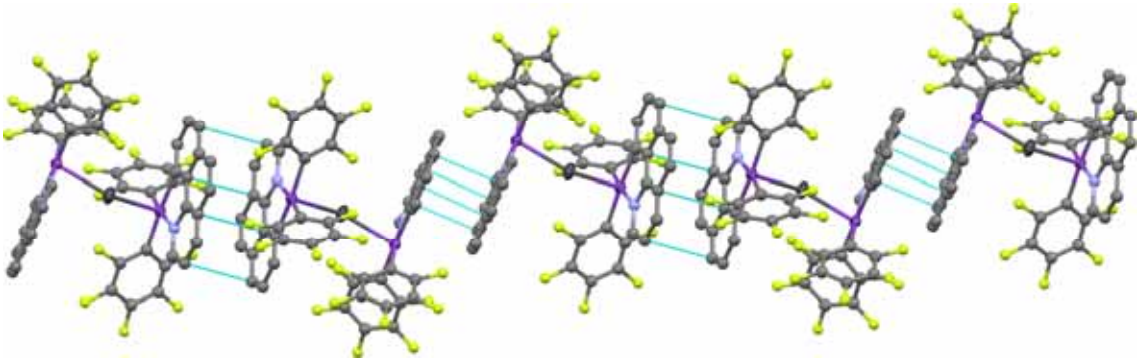

b

Figure 3. a) View of the molecular structure of [{Pt(bzq)(C_6F_5)$_2$}$_2$Pb] (**3**). Ellipsoids are drawn at their 50% probability level. b) Supramolecular arrangement in an infinite chain of **3**.

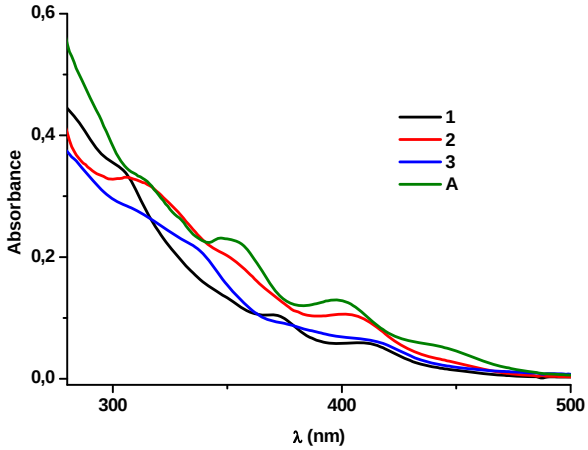

Figure 4. Absorption spectra of **1-3** and precursor **A** in THF 5×10^{-5} M at 298 K.

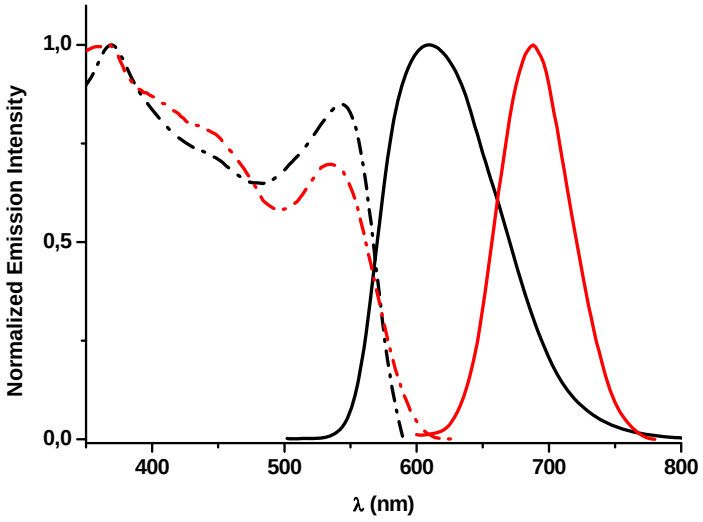

Figure 5. Normalized excitation and emission spectra of complex **1** in solid state at 298 K (black) and at 77 K (red) (λ_{exc} 400 nm).

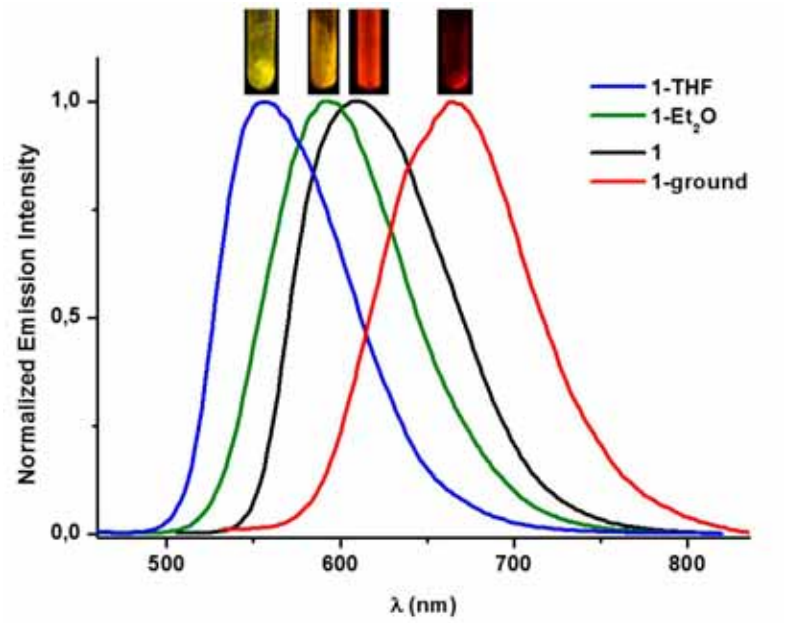

Figure 6. Normalized emission spectra of the orange-red solid **1**, **1-ground** and those of the fresh **1-THF** and **1-Et$_2$O** solvates.

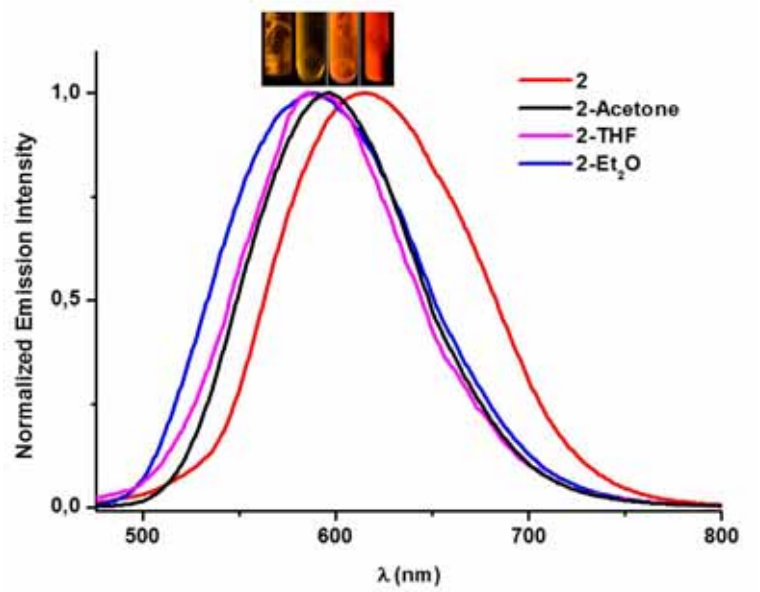

Figure 7. Normalized emission spectra of the orange solid **2** and of the solvates (**2-solvent**)

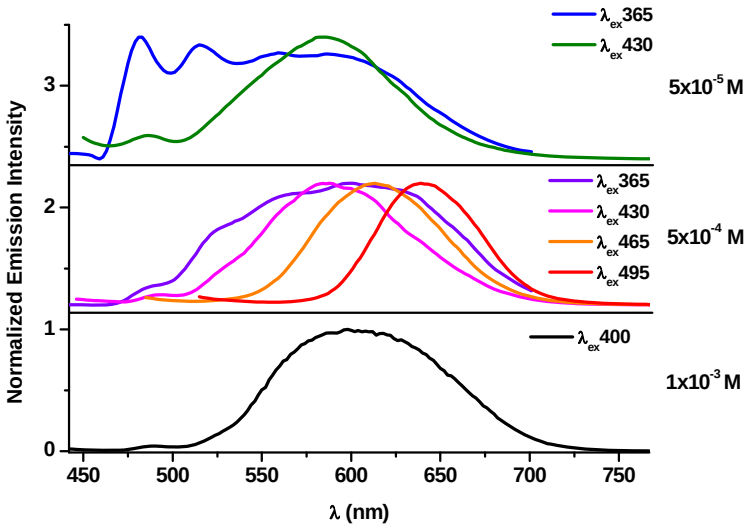

Figure 8. Normalized emission spectra of complex **1** in THF at 77 K at several concentrations (10^{-3}, 5×10^{-4} and 5×10^{-5} M) and using different excitation wavelengths.

Supporting Information

An extended Chain and Trinuclear Complexes Based on Pt(II)–M (M = Tl(I), Pb(II)) Bonds: Contrasting Photophysical Behaviour

Juan Forniés, Susana Ibáñez, and Antonio Martín*
Departamento de Química Inorgánica - Instituto de Síntesis Química y Catálisis Homogénea. Universidad de Zaragoza - C.S.I.C. 50009 Zaragoza, Spain

Nora Giménez, Elena Lalinde, and M. Teresa Moreno*
Departamento de Química-Centro de Síntesis Química de La Rioja, (CISQ), Universidad de La Rioja, 26006, Logroño, Spain.

Table S1. Selected bond lengths (Å) and angles (°) for $[\{Pt(bzq)(C_6F_5)_2\}Tl(Me_2CO)]_n \cdot n0.5Me_2CO \cdot n0.25n\text{-}C_6H_{14}$ (**1**$\cdot n0.5Me_2CO \cdot n0.25n\text{-}C_6H_{14}$)

Pt(1)–Tl(1)	2.9609(3)	Pt(1)–Tl(2)	2.9945(3)
Pt(2)–Tl(1')	2.9301(3)	Pt(2)–Tl(2)	3.0666(3)
Pt(1)–C(1)	2.026(6)	Pt(1)–C(7)	2.091(6)
Pt(1)–C(23)	2.070(5)	Pt(1)–N(1)	2.107(4)
Pt(2)–C(26)	2.064(7)	Pt(2)–C(32)	2.029(6)
Pt(2)–C(48)	2.050(9)	Pt(2)–N(2)	2.132(8)
Tl(1)–O(1)	2.805(6)	Tl(2)–O(2)	2.720(5)
C(1)–Pt(1)–C(23)	94.2(2)	C(1)–Pt(1)–C(7)	88.6(2)
C(23)–Pt(1)–C(7)	176.3(2)	C(1)–Pt(1)–N(1)	174.3(2)
C(23)–Pt(1)–N(1)	80.63(19)	C(7)–Pt(1)–N(1)	96.71(19)
C(1)–Pt(1)–Tl(1)	100.65(15)	C(23)–Pt(1)–Tl(1)	89.96(14)
C(7)–Pt(1)–Tl(1)	91.94(14)	N(1)–Pt(1)–Tl(1)	77.06(12)
C(1)–Pt(1)–Tl(2)	94.39(15)	C(23)–Pt(1)–Tl(2)	75.46(14)
C(7)–Pt(1)–Tl(2)	101.90(15)	N(1)–Pt(1)–Tl(2)	86.68(12)
Tl(1)–Pt(1)–Tl(2)	159.807(10)	C(32)–Pt(2)–C(48)	100.2(3)
C(32)–Pt(2)–C(26)	88.2(2)	C(48)–Pt(2)–C(26)	171.5(3)
C(32)–Pt(2)–N(2)	178.0(3)	C(48)–Pt(2)–N(2)	81.7(3)
C(26)–Pt(2)–N(2)	89.9(3)	C(32)–Pt(2)–Tl(1")	96.74(17)
C(48)–Pt(2)–Tl(1")	74.2(3)	C(26)–Pt(2)–Tl(1")	104.17(18)
N(2)–Pt(2)–Tl(1")	84.3(2)	C(32)–Pt(2)–Tl(2)	103.38(17)
C(48)–Pt(2)–Tl(2)	79.3(3)	C(26)–Pt(2)–Tl(2)	99.72(18)
N(2)–Pt(2)–Tl(2)	76.3(2)	Tl(1")–Pt(2)–Tl(2)	149.091(11)
Pt(2')–Tl(1)–Pt(1)	154.931(10)	Pt(1)–Tl(2)–Pt(2)	150.179(11)

The symmetry transformations used to generate equivalent atoms are –x+1/2, y+1/2, –z+3/2 for the primed atoms and -x+1/2, y-1/2, -z+3/2 for the doubly primed ones

Table S2. Selected bond lengths (Å) and angles (˚) for $(NBu_4)[\{Pt(bzq)(C_6F_5)_2\}_2Tl]$ as found in the forms **2a**, **2b** and **2c**

	2·0.75CH_2Cl_2 (**2a**)	**2**·CH_2Cl_2 (**2b**)	**2**·THF (**2c**)
Pt(1)–Tl	2.8815(4)	2.9254(3)	2.9352(6)
Pt(2)–Tl	2.9432(4)	2.8747(3)	2.9705(6)
Pt(1)–C(1)	2.021(10)	2.016(6)	2.016(4)
Pt(1)–C(7)	2.051(10)	2.077(5)	2.092(4)
Pt(1)–C(35)	2.068(9)	2.042(5)	2.053(4)
Pt(1)–N(1)	2.104(8)	2.088(5)	2.104(3)
Pt(2)–C(13)	2.031(8)	2.074(5)	2.047(4)
Pt(2)–C(19)	2.047(8)	2.024(5)	2.045(4)
Pt(2)–C(48)	2.051(8)	2.047(5)	2.092(4)
Pt(2)–N(2)	2.106(7)	2.075(5)	2.061(4)
Tl–O	-	-	2.630(4)
Pt(1)–Tl–Pt(2)	150.65(2)	146.91(1)	155.91(1)
C(1)–Pt(1)–C(7)	89.5(4)	87.5(2)	91.7(2)
C(1)–Pt(1)–C(35)	94.4(4)	94.3(2)	91.3(2)
C(7)–Pt(1)–C(35)	173.0(4)	174.9(2)	172.8(2)
C(1)–Pt(1)–N(1)	175.5(3)	174.1(2)	172.2(1)
C(7)–Pt(1)–N(1)	94.8(3)	97.5(2)	95.8(1)
C(35)–Pt(1)–N(1)	81.2(3)	80.4(2)	81.1(2)
C(1)–Pt(1)–Tl	101.6(3)	99.7(2)	105.11(11)
C(7)–Pt(1)–Tl	96.2(2)	98.6(1)	91.20(12)
C(35)–Pt(1)–Tl	88.7(2)	85.85(13)	94.37(11)
N(1)–Pt(1)–Tl	79.48(18)	82.73(12)	77.11(9)
C(13)–Pt(2)–C(19)	90.8(3)	88.9(2)	89.4(2)
C(13)–Pt(2)–C(48)	93.8(4)	175.2(2)	175.8(2)
C(19)–Pt(2)–C(48)	172.6(3)	94.8(2)	94.7(2)
C(13)–Pt(2)–N(2)	174.0(3)	95.8(2)	94.8(2)
C(19)–Pt(2)–N(2)	95.2(3)	173.7(2)	170.2(2)

C(48)–Pt(2)–N(2)	80.3(4)	80.3(2)	81.2(19)
C(13)–Pt(2)–Tl	102.3(2)	100.9(2)	102.6(1)
C(19)–Pt(2)–Tl	97.9(2)	96.9(2)	93.5(1)
C(48)–Pt(2)–Tl	86.8(2)	81.8(1)	76.8(1)
N(2)–Pt(2)–Tl	77.4(2)	86.4(1)	94.2(1)
O–Tl–Pt(1)	-	-	98.82(11)
O–Tl–Pt(2)	-	-	101.32(11)

Table S3. Selected bond lengths (Å) and angles (˚) for [{Pt(bzq)(C_6F_5)$_2$}$_2$Pb] (**3**)

Pt–C(1)	2.030(7)	Pt–C(7)	2.053(8)
Pt–C(23)	2.062(6)	Pt–N	2.090(7)
Pt–Pb	2.7757(3)		
C(1)–Pt–C(7)	89.4(3)	C(1)–Pt–C(23)	94.9(3)
C(7)–Pt–C(23)	174.8(3)	C(1)–Pt–N	173.4(2)
C(7)–Pt–N	94.9(3)	C(23)–Pt–N	80.5(3)
Pt'–Pb–Pt	150.26(2)		

The symmetry transformation used to generate the equivalent Pt' atom is -x+1/2, y, -z

Table S4. Photophysical data for complexes **1**-**3** in solution

Compound	Medium (T^a/K)	Color	λ^{em}_{max} /nm (λ_{ex})
[{Pt(bzq)(C_6F_5)$_2$}Tl(Me_2CO)]$_n$ **1**	THF 5×10^{-4} M (298)	yellow	490_{max}, 512, 580_{sh} (430)
	THF 10^{-3}M (77)	deep orange	600 (365-430)
	THF 5×10^{-4}M (77)	pale orange	485, 565, 600_{max}, 660_{sh} (365) 590 (430); 614 (465); 640 (495)
	THF 5×10^{-5}M (77)	white	480, 520, 580 (365) 590 (430)
	acetone 5×10^{-4} M (77)	pale orange	485, 520, 618_{max} (400) 620 (450)
	acetone 5×10^{-5} M (77)	white	485, 520, 565, 610_{sh} (365-430)
	CH_2Cl_2, 5×10^{-4} M (77)	purple	690 (400)
	CH_2Cl_2, 5×10^{-5} M (77)	pale-purple	480, 515, 602, 690_{max} (365) 602, 680 (440); 680 (530)
[{Pt(bzq)(C_6F_5)$_2$}$_2$Tl]$^-$ **2**	CH_2Cl_2, 5×10^{-4} M (298)	yellow	610 (400-460)
	CH_2Cl_2, 5×10^{-5} M (298)	yellow	600 (400-460)
	CH_2Cl_2, 5×10^{-4} M (77)	yellow	487_{sh}, 570_{max} (400-450)
	CH_2Cl_2, 5×10^{-5} M (77)	pale yellow	482, 520_{max}, 555_{sh} (400-420) 520_{max}, 555 (460)
[{Pt(bzq)(C_6F_5)$_2$}$_2$Pb] **3**	CH_2Cl_2 5×10^{-4} M (77)	orange	525, 570_{max} (420)
	CH_2Cl_2 5×10^{-5} M (77)	orange	525, 570_{max} (420)

Table S5. Crystal data and structure refinement for complexes [{Pt(bzq)(C_6F_5)$_2$}Tl(Me_2CO)]$_n$·n0.5Me_2CO·n0.25*n*-C_6H_{14} (**1**·n0.5Me_2CO·n0.25*n*-C_6H_{14}), (NBu_4)[{Pt(bzq)(C_6F_5)$_2$}$_2$Tl] (forms **2a**, **2b** and **2c**) and [{Pt(bzq)(C_6F_5)$_2$}$_2$Pb] (**3**).

	1·n0.5Me_2CO ·n0.25*n*-C_6H_{14}	**2**·0.75CH_2Cl_2 (**2a**)	**2**·CH_2Cl_2 (**2b**)	**2**·THF (**2c**)	**3**
formula	$(C_{28}H_{14}F_{10}NOPtTl)_n$ ·n0.5Me_2CO ·n0.25*n*-C_6H_{14}	$C_{66}H_{52}F_{20}N_3Pt_2Tl$ ·0.75CH_2Cl_2	$C_{66}H_{52}F_{20}N_3Pt_2Tl$ ·CH_2Cl_2	$C_{66}H_{52}F_{20}N_3Pt_2Tl$ ·THF	$C_{50}H_{16}F_{20}N_2PbPt_2$
M_t [g mol^{-1}]	1020.46	1925.35	1946.58	1933.76	1622.02
T [K]	100(1)	150(1)	100(1)	173(1)	100(1)
λ [Å]	0.71073	0.71073	0.71073	0.71073	0.71073
crystal system	monoclinic	monoclinic	monoclinic	orthorrombic	tetragonal
space group	$P2_1/n$	$P2_1/n$	$P2_1/c$	*Pbca*	$I4_1/acd$
a [Å]	13.5478(2)	15.6391(3)	13.6874(2)	20.8663(2)	31.0260(3)
b [Å]	22.9750(2)	21.9389(3)	19.5947(3)	20.2694(3)	31.0260(3)
c [Å]	20.6916(2)	21.3206(5)	24.0397(4)	31.1022(4)	20.8832(3)
β [º]	108.326(1)	109.132(3)	101.701 (2)	90	90
V [Å^3]	6113.82(12)	6911.1(2)	6313.47(17)	13154.6(3)	20102.4(4)
Z	8	4	4	8	16
ρ [g cm^{-3}]	2.217	1.850	2.048	1.953	2.144

μ [mm^{-1}]	9.925	6.517	7.156	6.791	9.006
F(000)	3796	3670	3712	7408	11968
2θ range [º]	7.6-52.5	7.6-50.2	7.5-57.7	2.6-54.9	7.4-50.1
no. of reflns collected	63265	37859	67324	193038	29605
no. of unique reflns	12298	12218	14747	14983	4444
R(int)	0.0340	0.0408	0.0490	0.0766	0.0502
final R indices [$I > 2\theta(I)$][a]					
R_1	0.0291	0.0412	0.0378	0.0306	0.0310
wR_2	0.0754	0.0994	0.0788	0.0588	0.0581
R indices (all data)					
R_1	0.0373	0.0784	0.0580	0.0567	0.0603
wR_2	0.0773	0.1145	0.0830	0.0655	0.0625
Goodness-of-fit on F^2[b]	1.021	1.026	1.016	1.020	1.029

[a] $R_1 = \sum(|F_o| - |F_c|) / \sum |F_o|$. $wR_2 = [\sum w (F_o^2 - F_c^2)^2 / \sum w(F_o^2)^2]^{1/2}$. [b] Goodness-of-fit = $[\sum w (F_o^2 - F_c^2)^2 / (n_{obs} - n_{param})]^{1/2}$.

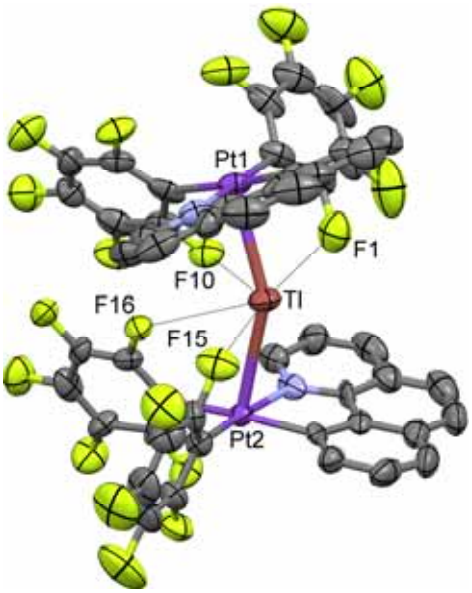

a

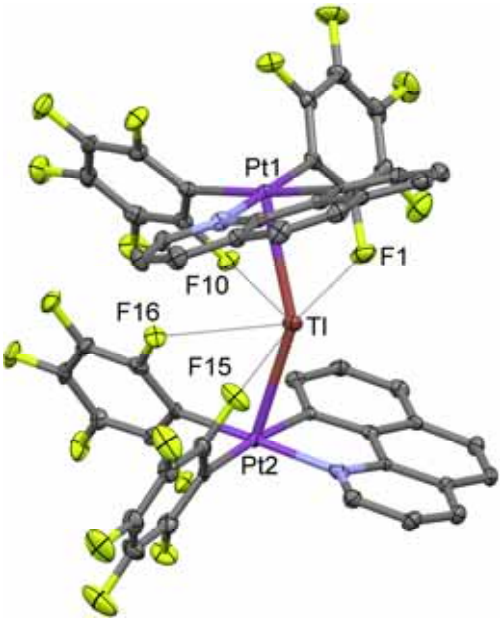

b

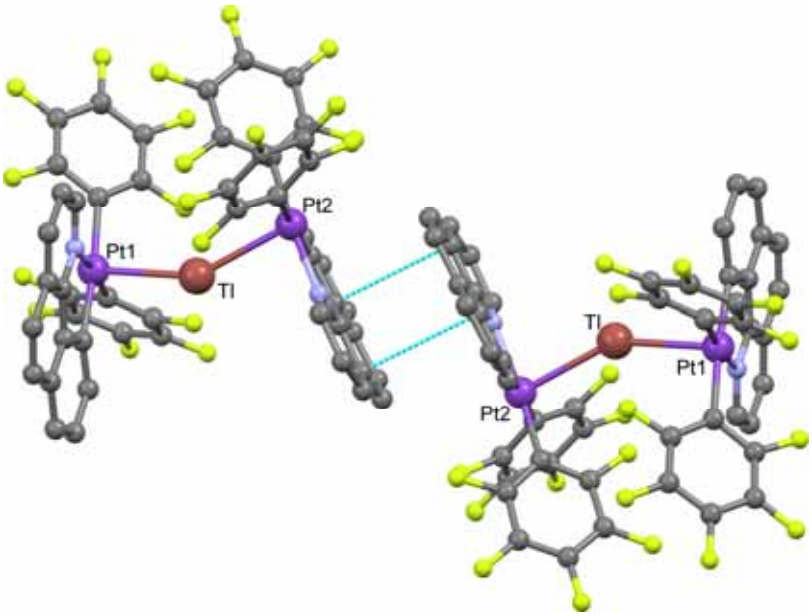

c

Figure S1. a, b) View of the molecular structures of **2a** and **2b**. Ellipsoids are drawn at their 50% probability level. c) Crystal packing of **2b**, showing the intermolecular contacts

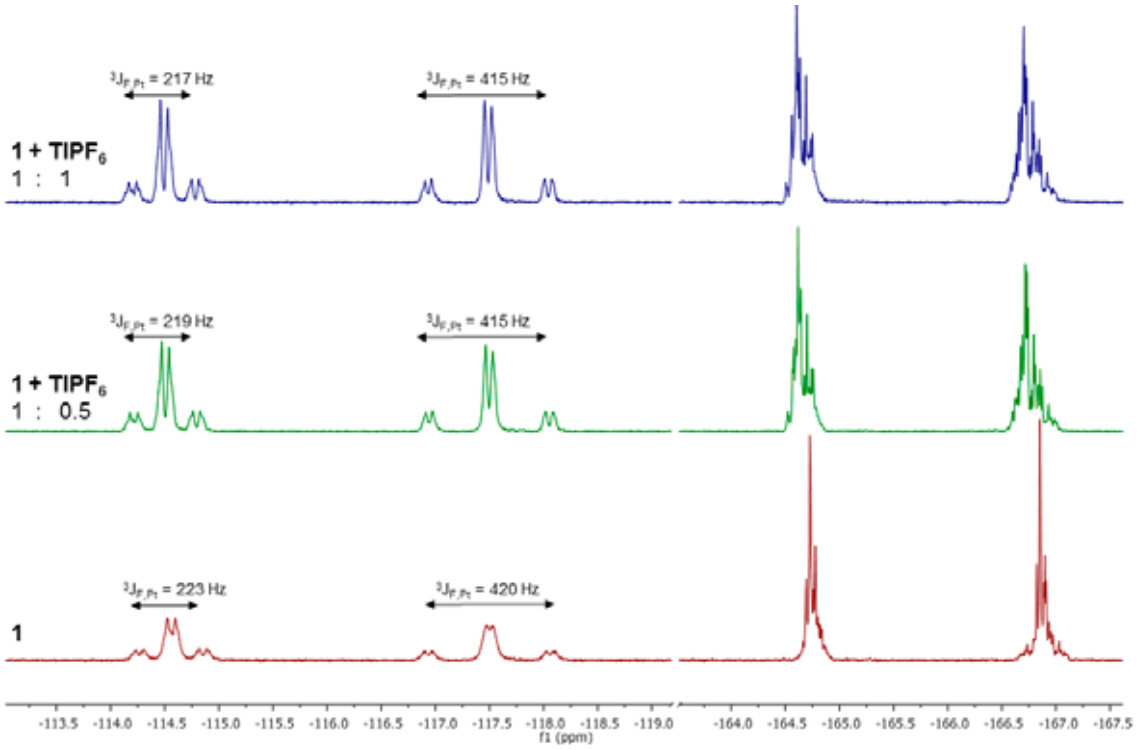

Figure S2. ^{19}F NMR spectra in CD_3COCD_3 of **1** and successive additions of $TlPF_6$ (molar ratio **1**:$TlPF_6$ 1:05 and 1:1)

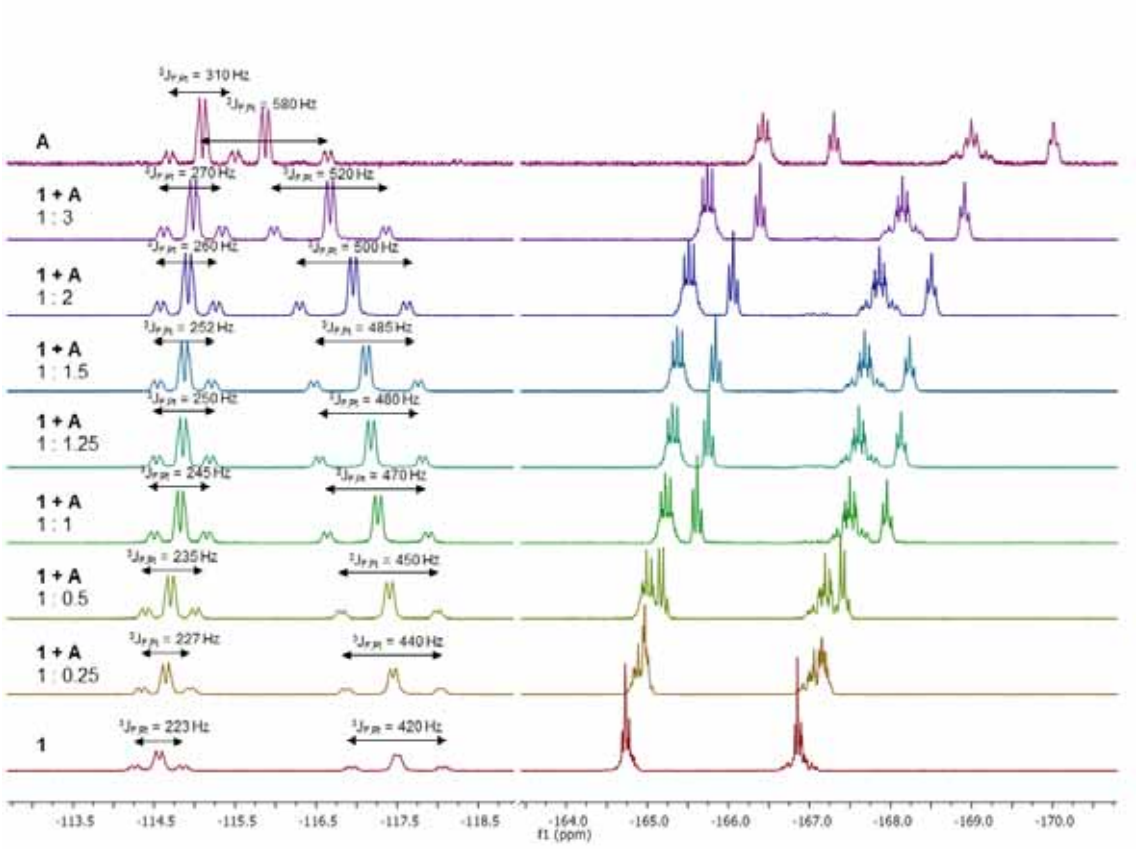

Figure S3. ^{19}F NMR spectra in CD_3COCD_3 of **1**, **A**, and successive additions of small amounts of **A** into a solution of **1**.

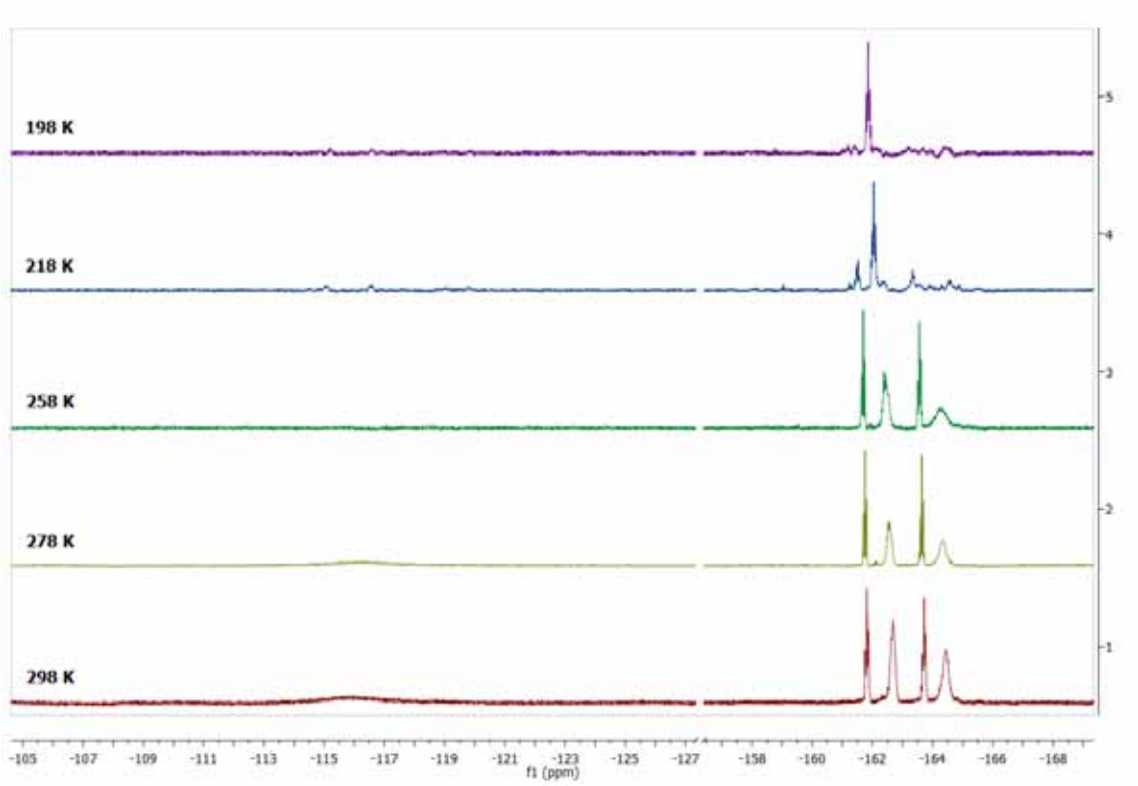

Figure S4. Variable temperature ^{19}F NMR spectra in CD_2Cl_2 of **1**

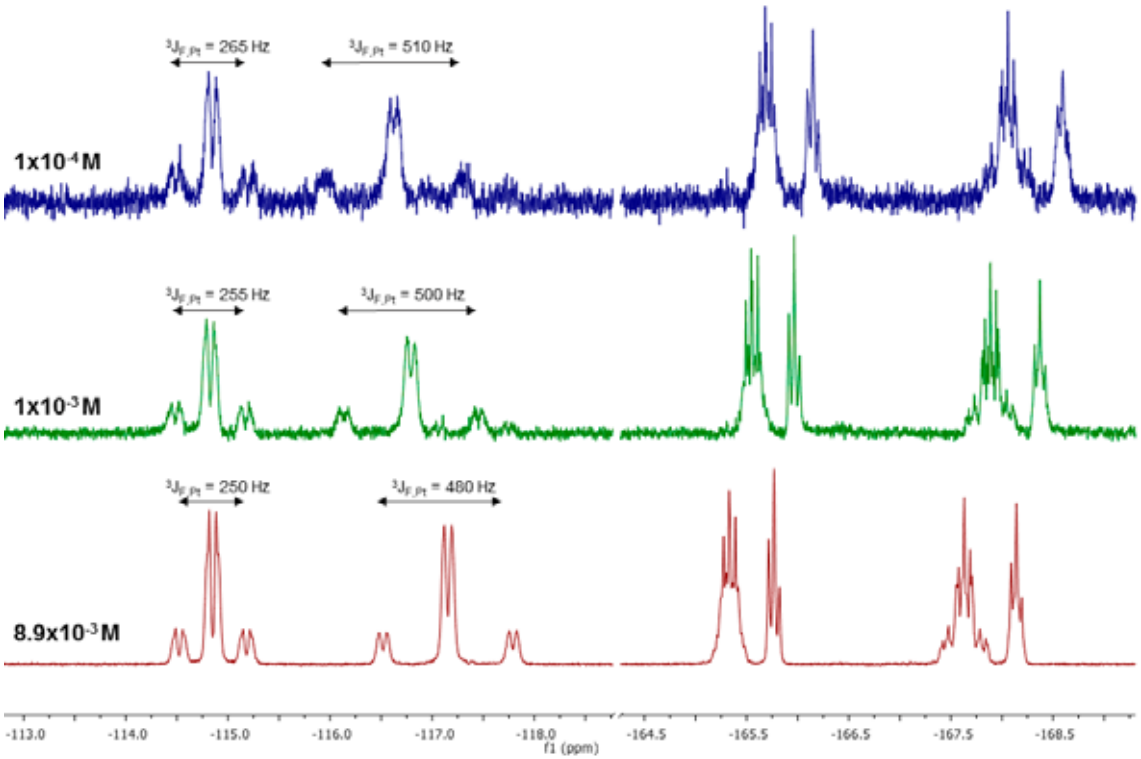

Figure S5. ^{19}F NMR spectra in CD_3COCD_3 of **2** at different concentrations (8.9×10^{-3} to 1×10^{-4} M) at 298 K.

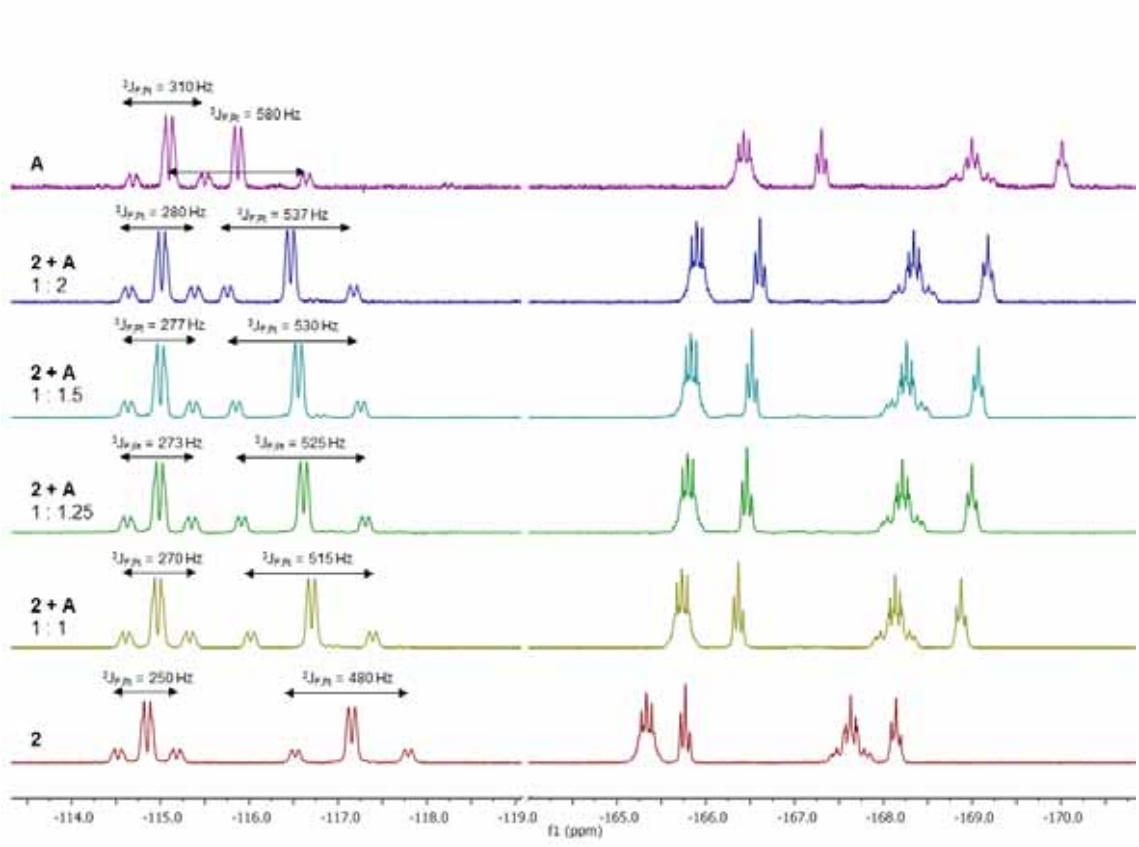

Figure S6. ^{19}F NMR spectra in CD_3COCD_3 of **2**, **A**, and successive additions of small amounts of **A** into a solution of **2**

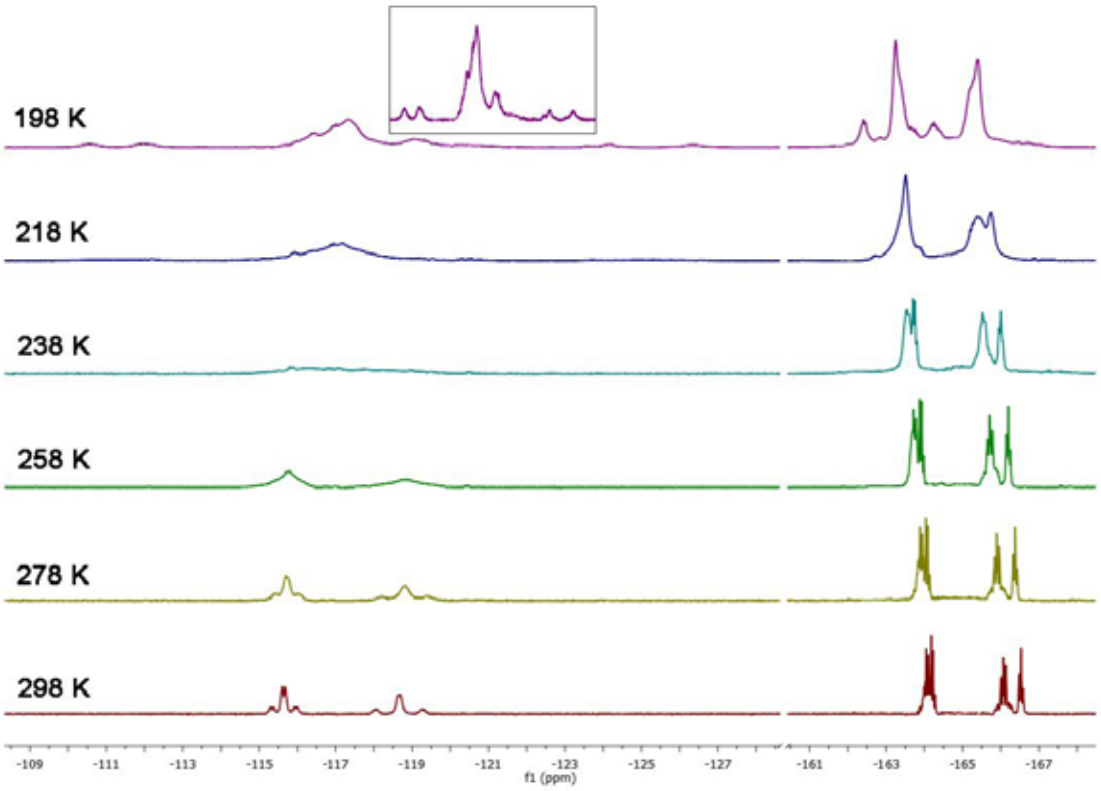

Figure S7. Variable temperature ^{19}F NMR spectra in CD_2Cl_2 of **2**

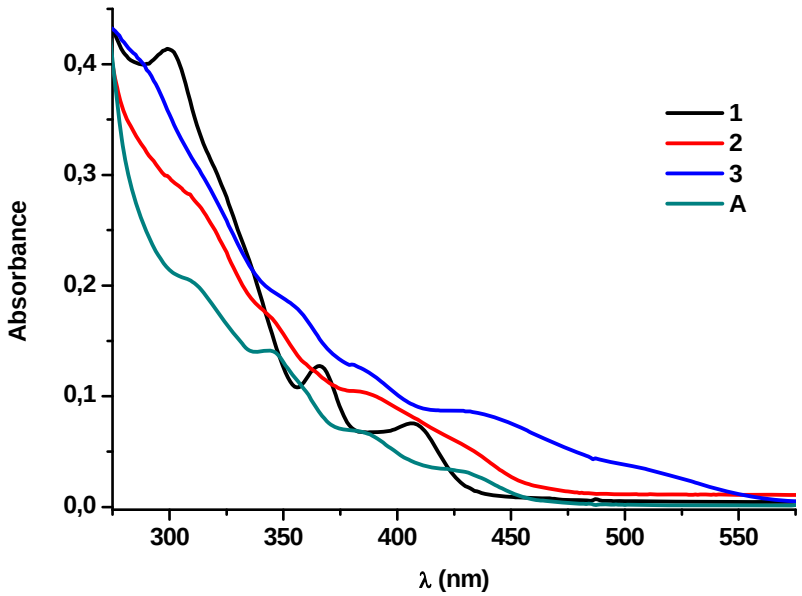

Figure S8. Absorption spectra of **1-3** and precursor **A** in CH_2Cl_2 5×10^{-5} M at 298 K.

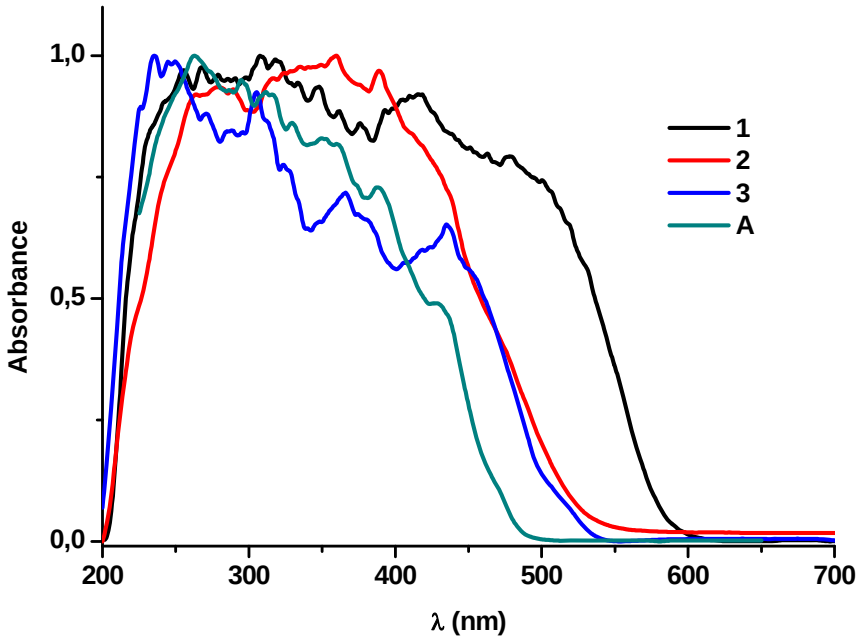

Figure S9. Normalized diffuse reflectance UV-vis spectra of **1-3** and the precursor **A** in the solid state.

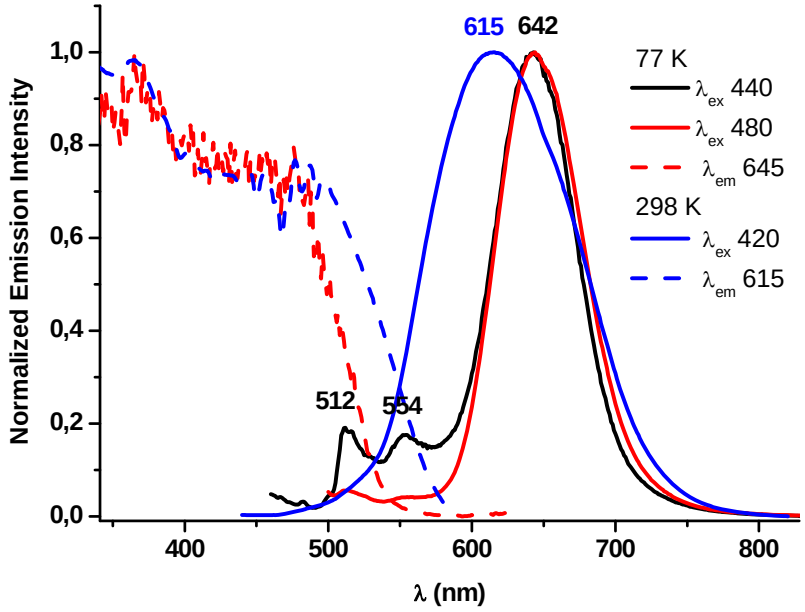

Figure S10. Normalized excitation and emission spectra of complex **2** in solid state at 298 K and at 77 K.

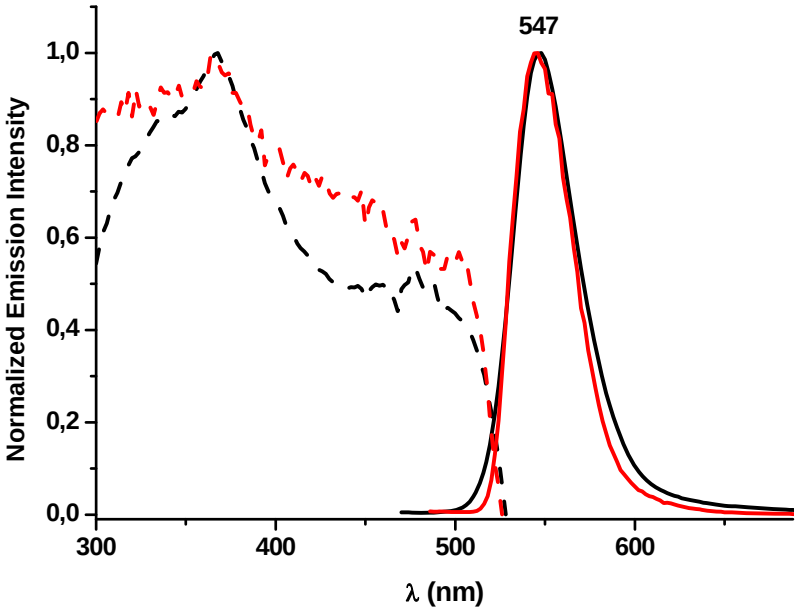

Figure S11. Normalized excitation and emission spectra of complex **3** in solid state at 298 K (black) and at 77 K (red) (λ_{ex} 400 nm).

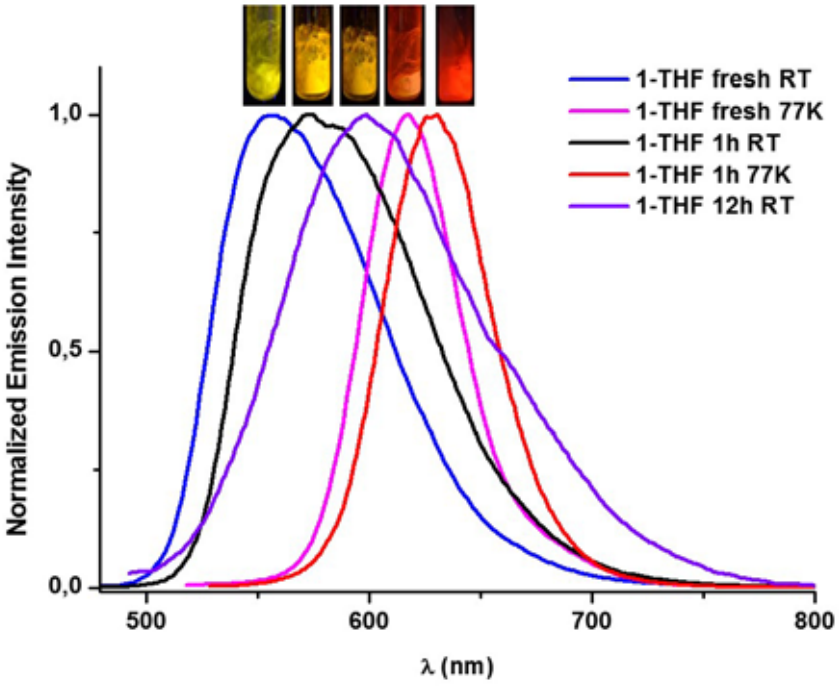

Figure S12. Normalized emission spectra of **1-THF** with the time under ambient conditions.

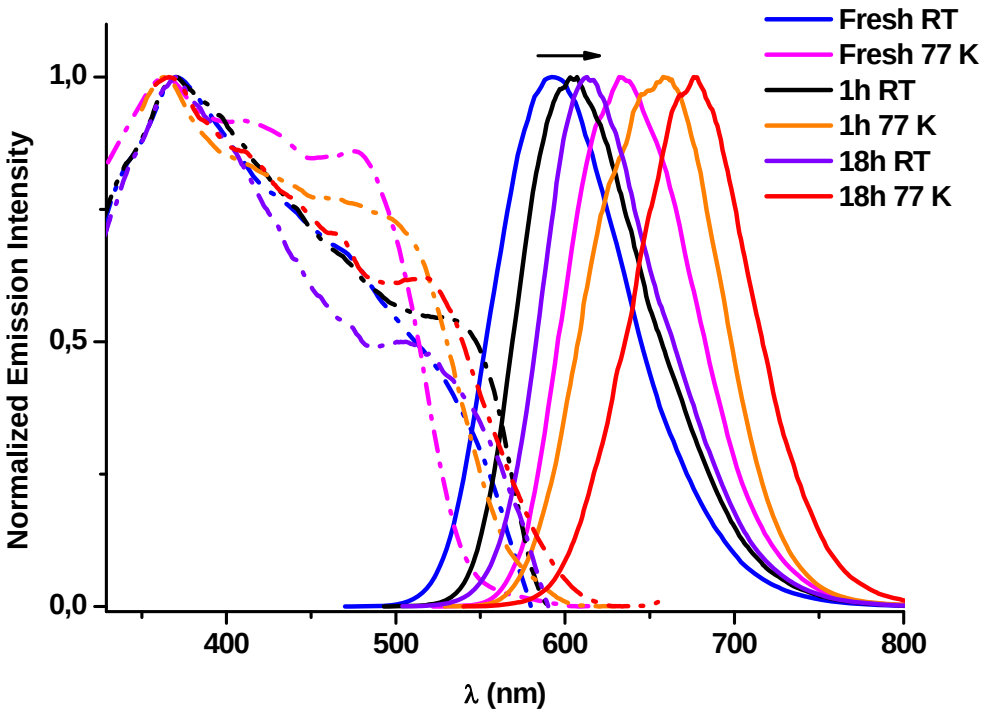

Figure S13. Normalized excitation and emission spectra of **1-Et$_2$O** with the time under ambient conditions

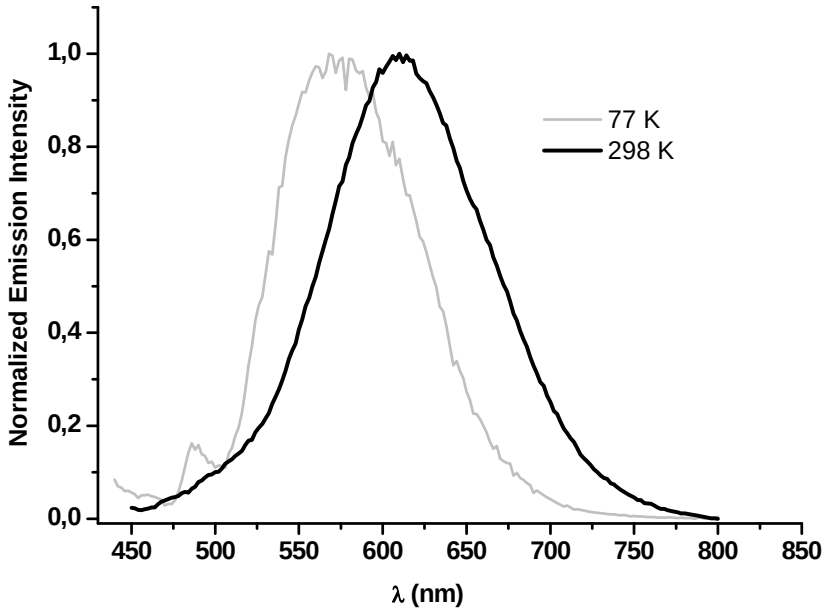

Figure S14. Normalized emission spectra of **2** in CH_2Cl_2 5 × 10^{-4} M (λ_{exc} 420 nm) at 298 K and at 77 K.

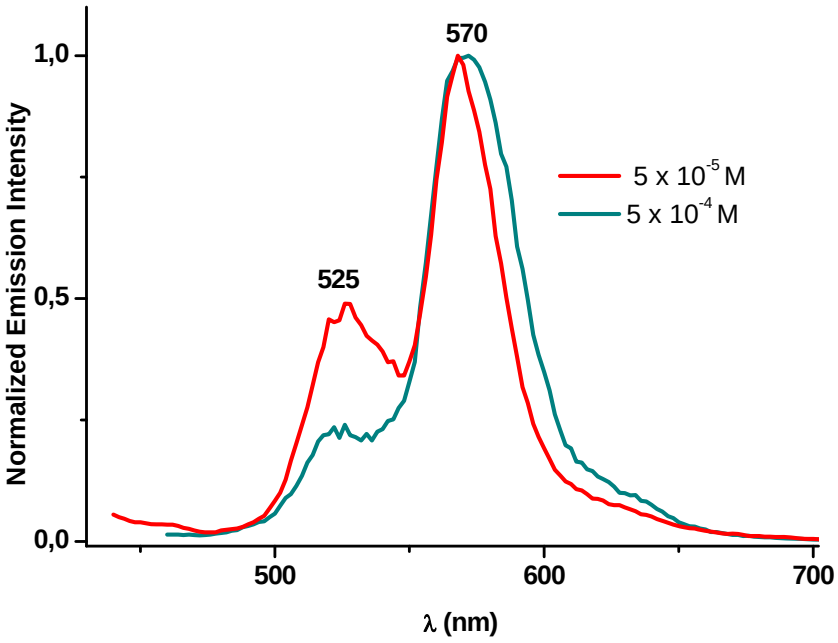

Figure S15. Normalized emission spectra of **3** in CH_2Cl_2 5×10^{-5} and 5×10^{-4} M (λ_{exc} 420 nm) at 77 K.